TOPICAL REVIEW — Magnetism, magnetic materials, and interdisciplinary research

Magnetic iron oxide nanoparticles: Synthesis and surface coating techniques for biomedical applications*

Sun Sheng-Nan(孙圣男)[a], Wei Chao(魏 超)[a], Zhu Zan-Zan(朱赞赞)[b], Hou Yang-Long(侯仰龙)[c], Subbu S Venkatraman[a]†, and Xu Zhi-Chuan(徐梽川)[a]‡

[a] School of Materials and Science Engineering, Nanyang Technological University, Singapore 639798, Singapore
[b] Department of Chemical Engineering, Worcester Polytechnic Institute, Worcester, MA 01609, United States
[c] Department of Materials Science and Engineering, College of Engineering, Peking University, Beijing 100871, China

(Received 2 January 2014; published online 24 January 2014)

Iron oxide nanoparticles are the most popular magnetic nanoparticles used in biomedical applications due to their low cost, low toxicity, and unique magnetic property. Magnetic iron oxide nanoparticles, including magnetite (Fe_3O_4) and maghemite (γ-Fe_2O_3), usually exhibit a superparamagnetic property as their size goes smaller than 20 nm, which are often denoted as superparamagnetic iron oxide nanoparticles (SPIONs) and utilized for drug delivery, diagnosis, therapy, and etc. This review article gives a brief introduction on magnetic iron oxide nanoparticles in terms of their fundamentals of magnetism, magnetic resonance imaging (MRI), and drug delivery, as well as the synthesis approaches, surface coating, and application examples from recent key literatures. Because the quality and surface chemistry play important roles in biomedical applications, our review focuses on the synthesis approaches and surface modifications of iron oxide nanoparticles. We aim to provide a detailed introduction to readers who are new to this field, helping them to choose suitable synthesis methods and to optimize the surface chemistry of iron oxide nanoparticles for their interests.

Keywords: Fe_3O_4, γ-Fe_2O_3, synthesis, surface coating, biomedical application

PACS: 75.47.Lx, 75.75.Cd, 61.46.–w, 81.16.Be **DOI:** 10.1088/1674-1056/23/3/037503

1. Introduction

Iron oxide nanomaterials have attracted great attention from many research fields. They have been found highly applicable and versatile in lithium ion batteries,[1] supercapacitors,[2] catalysis,[3] tissue-specific releasing of therapeutic agents,[4] labeling and sorting of cells,[5] as well as the separation of biochemical products.[6,7] Due to their superparamagnetic property and low toxicity, magnetic iron oxide (Fe_3O_4 and γ-Fe_2O_3) nanoparticles are especially interesting to biomedical applications, such as diagnostic magnetic resonance imaging (MRI),[8] thermal therapy,[9,10] and drug delivery.[8,11] For these applications, Fe_3O_4 and γ-Fe_2O_3 nanoparticles are usually smaller than 20 nm, where they exhibit superparamagnetic properties, i.e. a high magnetic saturation moment and nearly zero coercivity at room temperature. The external magnetic field can readily induce magnetic iron oxide nanoparticles towards magnetic resonance, self-heating, and also moving along the field attraction. These behaviors actually highly depend on the quality of the iron oxide nanoparticles, such as crystallization, size, and shape. It indicates the importance of synthesis approaches of iron oxide nanoparticles, i.e. the synthesis approaches that can produce well-crystallized and size-controlled iron oxide nanoparticles offer more opportunities for these applications. On the other hand, after synthesis, iron oxide nanoparticles need surface modification to make them more compatible in bio-systems for molecular conjugation and functionalization. They also often suffer from the chemical corrosion-induced instability. Therefore, the surface modification is a critical post-synthesis step for making iron oxide nanoparticles bio-compatible and stable. Some modifications also introduced additional chemical and/or physical properties onto iron oxide nanoparticles. In this review, we will focus on the synthesis approaches and surface modification techniques of magnetic iron oxide nanoparticles. A detailed comparison of the available physical and chemical synthesis methods is given, aiming to help readers who are new to this field to choose appropriate suitable synthesis methods for their research interests. The surface modification is given with inorganic and organic coatings. The advantages of surface modification are demonstrated with several MRI and drug delivery examples. In addition, we also give a brief introduction on crystal structure of Fe_3O_4 and γ-Fe_2O_3, size-dependent magnetism, and the working principles of magnetic nanoparticles in MRI.

*Project supported by Start-up Grant of Nanyang Technological University and Tier 1 Grant of Ministry of Education, Singapore (RGT8/13).
†Corresponding author. E-mail: assubbu@ntu.edu.sg
‡Corresponding author. E-mail: xuzc@ntu.edu.sg
© 2014 Chinese Physical Society and IOP Publishing Ltd

2. Fe_3O_4 and γ-Fe_2O_3

For Fe_3O_4 and γ-Fe_2O_3, the electron configuration of the Fe^{3+} ion is $1s^2 2s^2\ 2p^6\ 3s^2 3p^6 3d^5$ and Fe^{2+} ion is $1s^2\ 2s^2\ 2p^6\ 3s^2\ 3p^6\ 3d^6$. It is the Fe 3d electrons that determine the electronic, magnetic and some spectroscopic properties. In the ground state Fe^{3+} has five unpaired electrons and Fe^{2+} has two paired and four unpaired electrons. Magnetite, Fe_3O_4, is a ferrimagnetic oxide with a high Curie temperature ($T_C = 858$ K). It is in an inverse spinel structure with a face-centered cubic (fcc) unit cell (unit cell length $a = 0.839$ nm) based on 32 O^{2-} ions regularly cubic close packed along the [111] direction. There are eight formula units per unit cell. Fe_3O_4 chemically contains both Fe^{2+} and Fe^{3+}. The structure consists of octahedral and mixed tetrahedral/octahedral layers stacked along [111]. The formula can be written as $Fe^{3+}(A)[Fe^{2+}Fe^{3+}](B)O_4$. A is the tetrahedral site which is occupied by Fe^{3+} ions surrounded by four O atoms, while B is the octahedral site which is a mixture of Fe^{2+}/Fe^{3+} ions surrounded by six O atoms. Thus, Fe^{3+}occupies both tetrahedral and octahedral sites.[12,13] Fe atoms in A and B sites are coupled antiferromagnetically and the Fe^{2+} ions in B site contribute to macroscopic ferromagnetic properties.[14] As shown in Fig. 1, the magnetic properties of Fe_3O_4 are ascribed to the splitting of the 5d orbitals. The 5d orbitals are split into two subsets due to the oxide ligands and all Fe^{3+} and Fe^{2+} ions have four unpaired electrons, respectively. As can be seen, in the octahedral site, Fe^{3+} and Fe^{2+} ions are coupled ferromagnetically through a double exchange mechanism. The electron with the spin directing in the opposite direction of the others (in red), can be exchanged between two octahedral coordination sites. On the other hand, the Fe^{3+} ions in tetrahedral and octahedral sites are coupled antiferromagnetically via the oxygen, implying that the Fe^{3+} spins cancel out each other and thus merely unpaired spins of Fe^{2+} in octahedral coordination contribute to the magnetization. Fast electron hopping between the Fe^{3+} and Fe^{2+} ions at the B sites can lead to the Fe_3O_4 conductivity.[15] The Fe_3O_4 can be treated as half metal: a full spin polarization coming from the negative electron spin polarization at the Fermi level.[16,17] Maghemite, (magnetite-hematite), γ-Fe_2O_3, is also a ferrimagnetic oxide, whose structure ($a = 0.834$ nm) is similar to that of magnetite.[18] The difference between γ-Fe_2O_3 and Fe_3O_4 lies in all or most of Fe in γ-Fe_2O_3 is in the Fe^{3+} state and the oxidation of Fe^{2+} is compensated by cation vacancies. The unit cell contains 32 O^{2-} ions, 64/3 Fe^{3+} ions and 7/3 vacancies. Each cation occupies the tetrahedral site and the remaining cations are randomly distributed among the octahedral sites. The vacancies are usually confined to the octahedral sites.

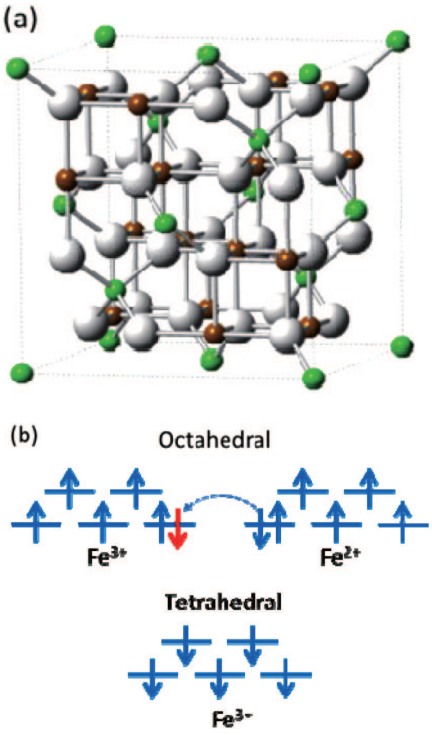


Fig. 1. (a) Crystal structure of Fe_3O_4, where green atoms are Fe^{2+}, brown atoms are Fe^{3+}, and white atoms are O.[18] (b) The electron, colored red, whose spin directs in the opposite direction of the others, can be exchanged between two octahedral coordination.

3. Size-induced magnetism evolution and application mechanisms

For all materials, the magnetism can be divided into five groups: diamagnetism, paramagnetism, ferromagnetism, antiferromagnetism, and ferrimagnetism. Diamagnetism is a basic property of all substances and it is a tendency to oppose an applied magnetic field. The magnetic susceptibility of a diamagnetic substance is small (-10^{-6}), negative and independent of temperature. The diamagnetic material has no unpaired electrons, and the paired electrons have opposite spin directions, so the magnetic moment will be offset. Paramagnetic substances have unpaired electrons whose spins have random magnetic moment directions. When applying a magnetic field, the spins will make themselves align to the applied magnetic field direction. The magnetic susceptibility is positive and small (0 to 0.01). It varies with temperature and its behavior is described by the Curie–Weiss law.[19] Ferromagnetic substances also have unpaired electrons, and they can also make their magnetic moments align to the applied magnetic field. The difference between paramagnetic and ferromagnetic substances lies in the magnetic moment of ferromagnetic substances will remain the lowered-energy state and parallel to each other, and this state can remain even though the applied magnetic field is removed. An antiferromagnet has a zero net moment because of the intrinsic magnetic moments of neighboring valence electrons having opposite directions. A ferrimagnet has two characters: 1) it can keep the magnetic

moment when lacking the magnetic field; and 2) neighboring pairs of electron spins are in the opposite directions. In the optimal arrangement, it will show more magnetic moment in one direction. The detailed magnetism classification can be found in the literature.[20]

Bulk Fe_3O_4 and γ-Fe_2O_3 are ferrimagnetic. They were classified as ferromagnetic materials a long time ago, before Néel's discovery of ferrimagnetism and antiferromagnetism in 1948.[21] The research in nanosized magnetic materials has found that the magnetism of materials is highly size-dependent.[22,23] The general rule is that as the size of ferromagnetic substances is sufficiently small, they will be like a single magnetic spin, which has a larger response to the applied magnetic field. Below such a size, the substances display the superparamagnetic property. Nanosized Fe_3O_4 and γ-Fe_2O_3 smaller than 20 nm are often considered in the range of a single domain and exhibit a superparamagnetic property. In the single-domain region, the coercivity decreases with the decrease of the particle size when the size is bigger than D_p (the superparamagnetic critical size). The coercivity will become zero when the particle size is smaller than D_p, which can be attributed to the randomization caused by thermal energy. There is a maximum coercivity that exists at the transition from multi-domains to a single-domain. In the multi-domain region, domain wall motion determines the magnetic property, and coercivity decreases when the overall size increases. When the nanoparticles are extremely small, the magnetic moment of nanoparticles is very small, and the magnetization will have a linear relationship with the magnetic field.[24] A high magnetic field will saturate the magnetization. Because of the fluctuation of magnetic moment caused by thermal energy, superparamagnetic nanoparticles do not present the remanence and coercivity.[24–27]

A major application of superparamagnetic iron oxide nanoparticles is magnetic resonance imaging (MRI). MRI is a medical imaging technique using a strong magnetic field and radio waves for body diagnosis. Because the human body is largely composed of water molecules containing protons, when the body is placed in the MRI scanner, the magnetic moments of protons will align to the applied magnetic field direction. If a radio frequency (RF) electromagnetic field is applied, proton magnetic moments will change. As this RF electromagnetic field is turned off, the magnetic moments will return to their original state. Most MRI applications rely on detecting a radio frequency signal emitted by excited protons. Since the time or rate of the protons in different tissues return to their equilibrium state after the microwave is removed are different, the diseased tissue can be detected. When the RF electromagnetic field is switched off, the flipped nuclear spins tend to return to a low energy state along the applied magnetic field and thus there will appear two independent processes: the spin-lattice relaxation T1 process and the spin-spin relaxation T2 process. They can be used to demonstrate different anatomical pathologies. In the T1 process, the magnetic moments will recover to the low energy state: aligned to the applied magnetic field direction, while in the T2 process, the magnetic moments will decay in the xy-plane perpendicular to the applied magnetic field direction. Thus, the image signal from the T1 process will be brighter because the magnetic moments in the applied magnetic field direction increase, while the image signal from T2 will be darker. In order to accelerate T1 and T2 processes and further increase the contrast, the contrast agents are desired to accelerate the relaxation. The contract enhancement can be measured by relaxation rate $R = 1/T$ (s^{-1}) and relaxivity $r = R$/concentration ($mM^{-1}\cdot s^{-1}$). If a higher relaxivity is obtained, an enhancement on contrast will be observed. Gd^{3+}-complexes often serve as the T1 contrast agent,[28,29] and magnetic nanoparticles (MNPs) are often used as the T2 contrast agent. The contrast effects are determined by $(M_sV)^2$ and d^{-6}, where M_s is the saturation magnetization, V is the volume of nanoparticles, and d is the distance from the MNP surface to the protons. Therefore, the magnetic nanoparticles with a high M_s, uniform size, and thin surface coating layer will be able to give a shaper contrast.[28,30,31] The synthesis and surface modification of magnetic nanoparticles for MRI purposes should follow this rule to reach a higher detection sensitivity.

In addition, because superparamagnetic iron oxide nanoparticles can be imaged in MRI and also be moved under an applied external magnet, they have great potential to be the carriers of drug molecules for targeted drug delivery. Ideally, the targeted drug delivery[32] technique delivers the medicine directly to the disease parts of a patient. It can increase the local medicine concentration and reduce the dosage intake by the patient. As a result, the usage of the drug can be more efficient with lower side-effects and fluctuation in circulating drug levels. Magnetic nanoparticles can be followed using MRI so that the transportation of the drug with magnetic carriers can also be tracked or guided.[33] Magnetic nanoparticles for drug delivery should not only meet the criteria of an MRI contrast agent, but also need carrying sites for the drug. Because of the limited space on the nanoparticle surface for both targeting agent and drug, surface coating/modification is a major approach for creating loading sites for carrying drugs.[34]

4. Synthesis approaches

4.1. Physical vapor deposition (PVD)

Physical vapor deposition is a vacuum deposition method used to deposit thin films by the condensation of a vaporized form of the desired material on the substrates. It is purely physical processes such as high-temperature vacuum evapo-

ration with subsequent condensation, or plasma sputter bombardment rather than a chemical reaction at the surface as chemical vapor deposition (CVD). Many research groups report to prepare iron oxides using PVD. Various PVD methods such as pulsed laser deposition (PLD),[35,36] reactive molecular beam epitaxy (MBE)[37] and sputtering[38,39] have conventionally been used to grow these spinel ferrites. For example, Boho *et al.* utilized the facing target sputter technique to make Fe_3O_4 epitaxial growth on MgO single crystal substrates.[40] Pandya *et al.* deposited Fe_3O_4 nanoparticle film on Si(100) using pulsed DC sputtering under the assistance of an electric field.[41] Since γ-Fe_2O_3 has almost the same lattice parameters to Fe_3O_4, XRD cannot distinguish the phase between Fe_3O_4 and γ-Fe_2O_3 alone. Some researchers used Raman spectra and Mössbauer spectroscopy to ensure the phase purity.[41] You *et al.* reported the preparation of iron/iron oxide core-shell nanoclusters via nanocluster deposition system, which employed a combination of magnetron sputtering and gas-aggregation techniques. The iron nanoparticles were prepared by passivating the Fe surface with MgO in order to retain the Fe high magnetic moments.[38] However, the method of growing γ-Fe_2O_3 nanoparticle films has been limited to reactive MBE and facing target sputtering.[39] Most recently, Yanagihara *et al.* prepared Fe_3O_4 and γ-Fe_2O_3 on single crystal MgO (001) using reactive sputtering. When the total gas pressure was 0.5 Pa, and the Ar flow rate was 30 sccm, changing the O_2 flow rate can be used to choose to grow Fe_3O_4 or γ-Fe_2O_3. When the O_2 flow rate is controlled between 0.2 sccm to 0.5 sccm, the product is Fe_3O_4; when the O_2 flow rate is bigger than 0.7 sccm, the product is γ-Fe_2O_3.[39]

4.2. Chemical vapor deposition (CVD)

Chemical vapor deposition was also reported for synthesizing Fe_3O_4 nanoparticles by some groups, but the reports are relatively rare. Rochel *et al.* used CVD to prepare carbon-coated Fe_3O_4 particles by the reduction of Fe_2O_3 in methane and nitrogen.[42] The carbon coating is commonly used because of its biocompatibility and chemical stability.[42] Recently, Mantovan *et al.* synthesized Fe_3O_4 thin film via CVD using $Fe(C_6H_8)(CO)_3$ as a precursor.[43] The method improved the stoichiometry degree as compared with carbonyl precursors.[43–45] The thickness of Fe_3O_4 can be controlled by varying CVD pulses. Because the limitation of approach, both PVD and CVD have been found to not be suitable for producing iron oxide in the nanoparticle form. Even some reports with nanoparticle formation, the post-synthesis treatments, such as scratching powders from substrates and dispersing in solvent by sonication or surface modification, have to be used. These shortcomings limit their biomedical applications in a wet-chemical environment.

4.3. Electrodeposition

Similar to vapor deposition, electrodeposition also involves the deposition of precursors onto a substrate to form nanostructures. But the electrodeposition usually can be conducted under room temperature with dissolved Fe^{2+} or Fe^{3+} ions as precursors. It is promising to prepare large-scale iron oxide nanomaterials.[46–50] Evidence from the literature suggests that, in general, changes in deposition potential and electrolyte composition can significantly affect film formation, including crystallinity, grain size, and orientation.[47] Carlier *et al.* prepared Fe_3O_4 by anodic oxidation of Fe^{2+} at 80 °C under N_2 atmosphere, and used KCH_3COO and $(NH_4)_2Fe(SO_4)\cdot 6H_2O$ as precursors. The gold-coated polycarbonate membrane served as templates.[51] Poduska *et al.* used the same precursor to prepare Fe_3O_4 on metal substrates (Fig. 2). The magnetic hysteresis response of Fe_3O_4 film can be tuned by changing the applied potential and electrolyte composition.[47] In addition, they found that acetate played an important role in controlling the ratios of Fe_3O_4 and γ-Fe_2O_3. At a higher concentration of acetate in the electrolyte, pure Fe_3O_4 can be produced.

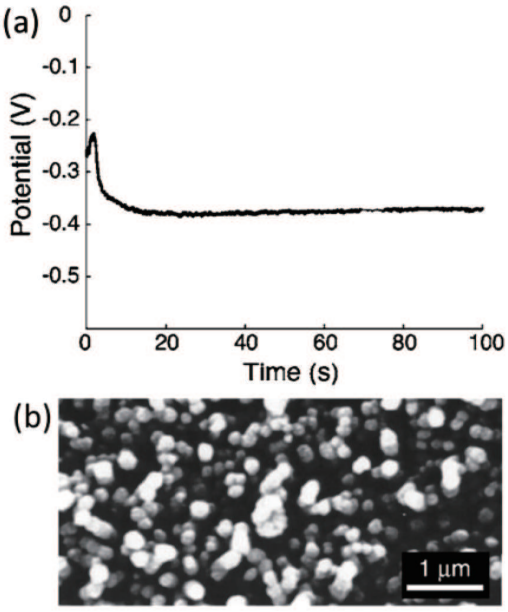


Fig. 2. (a) Applied deposition potential vs. time for a sample prepared galvanostatically at 50 μA/cm^2. Within the first 15 s of deposition, the applied potential stabilizes to a potential at which magnetite is electrodeposited, and no significant variation in potential is observed over 15–90 min of deposition. (b) Scanning electron micrographs show that rounded, columnar crystallites appear in deposits synthesized potentiostatically, in this case at −0.425 V vs. Ag/AgCl reference electrode (Fisher Scientific), from electrolytes with higher acetate concentrations.[47]

4.4. Hydrothermal

The hydrothermal is one of the most popular wet chemical approaches for synthesis of inorganic nanocrystals, especially for metals and metal oxides.[52,53] This method often

employs a relative high temperature and a high pressure to induce or affect the formation of nanocrystals. The solubility of reactants and desired products under such a condition is critical. Hydrothermal synthesis has various advantages such as high reactivity of the reactants, facile control of product morphology, and good crystallization of products. In addition, some metastable and unique condensed phases can also be produced under a high pressure condition. As for magnetic nanoparticles,[54] nanospheres,[52] nanosheets,[55] nanoplates,[56,57] nanorods,[58,59] nanocubes,[60] nanorings,[61] nanowires,[62] etc. have been successfully synthesized by the hydrothermal synthetic method.[63] Chen *et al.* prepared quasi-sphere polyhedron nanoscystalline Fe_3O_4 nanoparticles with an average of 50 nm by the hydrothermal method. They employed $Na_2S_2O_3$ as the phase control agent. The ratio of $Na_2SO_3/FeSO_4$ determined whether the Fe_3O_4 phase can be produced.[64] Date *et al.* prepared spherical Fe_3O_4 with a size range of 150–200 nm using microwave hydrothermal reaction in 90–200 °C. The $FeSO_4{\cdot}7H_2O$ and $FeCl_3$ served as precursors and NaOH was used as the hydrolysis reactant. It was found that Fe/NaOH was a critical parameter to control Fe_3O_4 formation. As compared with other hydrothermal methods, the microwave facilitates the kinetics of reaction.[65] Different from reducing the Fe^{3+} precursor, Chen *et al.* prepared Fe_3O_4 nanopowders via a hydrothermal process using Fe^{2+} precursor ($FeCl_2{\cdot}4H_2O$). They used the mixture of NaOH and N_2H_4 to react with $FeCl_2$. N_2H_4 was believed as an oxidant to partially oxidize Fe^{2+} to Fe^{3+}.[66] Zheng *et al.* reported the synthesis of octahedral-like Fe_3O_4 nanoparticles using EDTA-assisted in mild condition. The starting reactants are $FeCl_3$, $H_2H_4{\cdot}H_2O$ and NaOH and EDTA. The EDTA acted as a surfactant and assisted the shape control.[54] Polyvinylpyrrolidone (PVP) was also used as the surfactant in the hydrothermal method. It was reported that by mixing $FeCl_3$, $FeSO_4{\cdot}7H_2O$, NaOH with PVP and benzene, the shape of the Fe_3O_4 nanoparticles can be controlled. By varying experimental conditions and the amount of PVP, different morphologies of Fe_3O_4 can be obtained, such as nanoparticles, nanowires, bundles, and nanorods.[67] A further study revealed that hexagonal, dodecahedral, truncated octahedral and octahedral shapes can also be synthesized by modifying this method. The modification on the recipe was mainly made on the surfactant and precipitation agent selection. L-arginine and CTAB were used as the precipitation agent and surfactant, respectively.[68] Another similar modification was reported by Gai *et al*. They used $FeSO_4{\cdot}7H_2O$, polyethylene glycol (PEG), NaOH, and KNO_3 to synthesize octahedral Fe_3O_4 with the size of 200–300 nm. It was found that the ratio of PEG and NaOH was important to the formation of octahedral Fe_3O_4 nanoparticles (Fig. 3). If a higher concentration of NaOH was employed, PEG would prefer to adsorb on the (111) plane of Fe_3O_4 and decrease the growing rate along the [111] axis.[69]

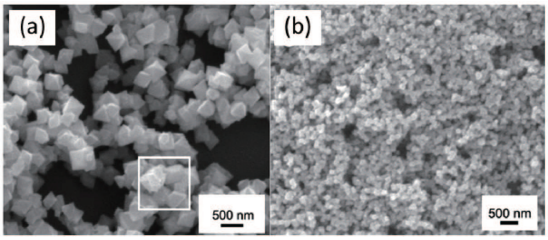


Fig. 3. SEM images of the Fe_3O_4 samples prepared (a) with and (b) without PEG-6000.[69]

4.5. Co-precipitation

Co-precipitation is widely used in the aqueous phase synthesis of Fe_3O_4 nanoparticles.[70] In general, the method employs an alkaline solution, such as NaOH and $NH_3{\cdot}H_2O$, to precipitate Fe^{2+} and Fe^{3+} ions in an aqueous solution. The Fe_3O_4 nanoparticles were produced by dehydration from the intermediate iron hydroxides. The surfaces of so-produced iron oxide nanoparticles are rich in OH group and the nanoparticles can be suspended well in an aqueous solution.[71–73] Refait and Olowe found another formation mechanism that $Fe(OH)_2$ can also serve as an intermediate for Fe_3O_4 formation. The mechanism includes the precipitation of Fe^{2+} by alkaline, the oxidation of $Fe(OH)_2$ by O_2 in air to FeOOH, and the combination of $Fe(OH)_2$ and FeOOH to form Fe_3O_4.[74–76] It indicated that if only Fe^{2+} was used as the precursor, the co-precipitation method under air could still produce Fe_3O_4 nanoparticles and thus there was potentially no need to involve Fe^{3+} as precursors.

Gao *et al.* used $C_6H_5Na_3O_7{\cdot}2H_2O$, NaOH, $NaNO_3$, $FeSO_4{\cdot}4H_2O$ in an aqueous solution to prepare Fe_3O_4 nanoparticles on the gram scale. The diameter range of Fe_3O_4 nanoparticles can be tuned from ∼20 nm to 40 nm (Fig. 4) by changing the experimental parameters. The citrate ions served as the surfactant, which capped on the surface of Fe_3O_4 nanoparticles and prevented them from aggregation by the repulsive force between radical ions.[76] In 2012, Mo *et al.* prepared Fe_3O_4 by injecting $NH_3{\cdot}H_2O$ into the Fe^{3+} and Fe^{2+} aqueous solution under ultrasonic conditions.[77] Ahmad *et al.* prepared Fe_3O_4 on the exterior surface layer of talc mineral by co-precipitation of $FeCl_2$ and $FeCl_3$ in NaOH aqueous solution.[78] In 2012, Xia *et al.* reported a novel complex-coprecipitation method to synthesize Fe_3O_4 nanoparticles. They used triethanolamine [$N(CH_2CH_2OH)_3$, TEA] as ligands to govern the quality of the Fe_3O_4nanoparticles. The readily available and cost-effective iron precursors, $Fe_2(SO_4)_3$ and $FeSO_4$, were used to synthesize the TEA-coated Fe_3O_4 nanocrystals. TEA played a role in limiting the Fe_3O_4 growing rate due to its chelation to Fe^{3+} and Fe^{2+}. Additionally, TEA can prevent the Fe_3O_4 from agglomeration due to

the TEA molecules being rooted in the colloid particles.[79] Co-precipitation was also reported for the shape control on Fe_3O_4 nanoparticles. Yan *et al.* reported the synthesis of Fe_3O_4 nanowires through NaAc-assisted co-precipitation in an aqueous solution with $FeSO_4{\cdot}7H_2O$, NaAc, and NaOH. The morphology could be controlled by altering the concentration of NaAc.[80] However, because of a polarized environment, the weak bonding between capping agents and the iron oxide surface was often interrupted by the hydrogen bond interactions between the iron oxide surface and the water solvent. It resulted in a limited control over the size and shape in co-precipitation approach.

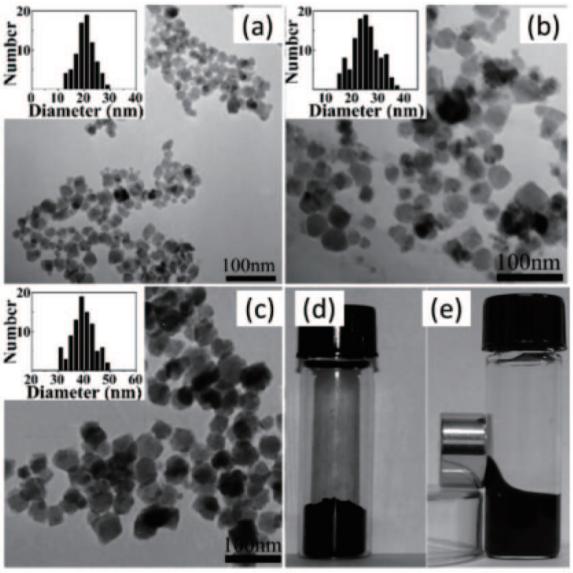


Fig. 4. (a)–(c) TEM images and size distributions of Fe_3O_4 nanoparticles synthesized by co-precipitation in the presence of sodium citrate with the different mean diameters of 20 nm ((a), $\sigma = 16\%$), 25 nm ((b), $\sigma = 19\%$), and 40 nm ((c), $\sigma = 10\%$). (d) As-synthesized hydrophilic Fe_3O_4 nanoparticles in powder form. (e) Fe_3O_4 nanoparticles dispersed in water, which can be attracted by a magnet.[76]

4.6. High-temperature (thermal) decomposition of organometallic precursors

As stated above, for the co-precipitation route, it is difficult to optimize the size and size distribution of nanoparticles. It is also difficult to achieve high crystalline or control the particle shape. This is because the most co-precipitation reactions occur at low temperature and their chemical reaction kinetics can be only controlled by adding rate of reactants. It results in limited control over nucleation and growth. The lack of capping agent also results in the difficulty of size control. In addition, the crystallization is usually improved by temperature. The synthesis temperature of co-precipitation in aqueous solution is limited by the low boiling point of aqueous solution and thus so-produced iron oxide nanoparticles are in low crystallization. Thus, it is desirable to develop some high temperature synthesis approaches to prepare high quality Fe_3O_4 nanoparticles.[79]

In recent years, thermal decomposition of organometallic precursors, such as $Fe(acac)_3$ and Fe-oleate, has been found to be one of the best approaches to produce magnetic iron oxide nanoparticles for biomedical applications.[28,81,82] The iron oxide nanoparticles produced by this method are usually well-controlled in size and shape. Due to the high temperature, nanoparticles are also well crystallized with a high saturation moment. The first report using thermal decomposition of $Fe(acac)_3$ was made by Sun *et al.* in 2002.[15] The method involved the thermal decomposition of $Fe(acac)_3$ in the presence of surfactants, oleylamine and oleic acid. To partially reduce Fe^{3+} to Fe^{2+}, a reducing agent 1,2-hexadecanediol was also used. To achieve the high temperature, organic solvents with high boiling point (> 250 °C) of phenyl ether or benzyl ether were used. The method produced Fe_3O_4 nanoparticles confirmed by XRD and Mossbauer spectroscopy. The size could be controlled between 4–16 nm (Fig. 5) and the size of nanoparticles was uniform. By a thermal treatment in O_2, Fe_3O_4 nanoparticles could be converted to γ-Fe_2O_3.[15]

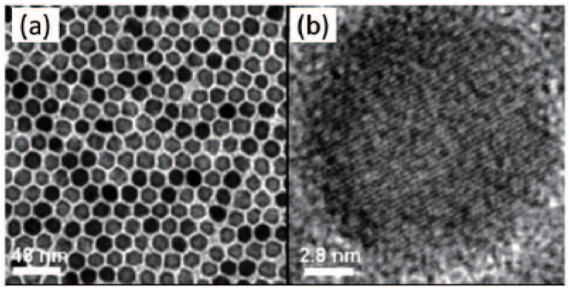


Fig. 5. (a) TEM image of 16-nm Fe_3O_4 nanoparticles synthesized by thermal decomposition of $Fe(acac)_3$ in the presence of oleic acid and oleylamine. (b) HRTEM image of a single Fe_3O_4 nanoparticle.[15]

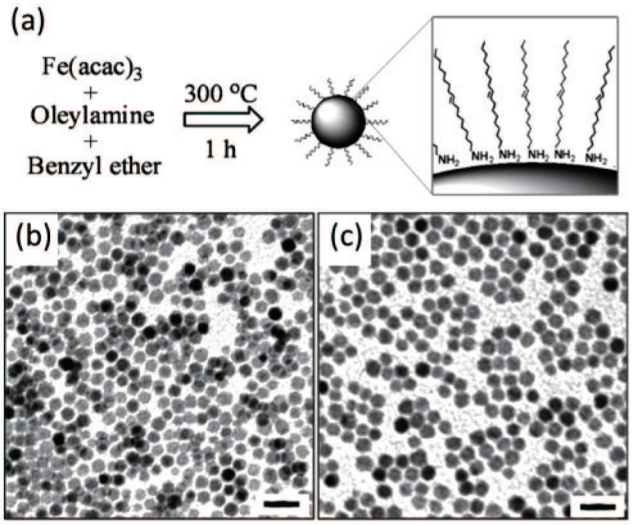


Fig. 6. (a) The modified recipe for synthesizing Fe_3O_4 nanoparticles capped only by oleylamine. TEM images of as-synthesized Fe_3O_4 nanoparticles using (b) only oleylamine and (c) a mixture of oleylamine and benzyl either.[83]

This thermal decomposition method was further simplified by Xu *et al.* in 2009. It was found that oleylamine could

serve as the solvent, surfactant, and reducing agent. Therefore, the recipe could be simplified to use two or three chemicals. As illustrated in Fig. 6,[83] Fe_3O_4 nanoparticles were synthesized by heating a mixture of $Fe(acac)_3$, oleylamine, and benzyl ether. The decomposition of $Fe(acac)_3$ was found beginning since 250 °C, where the nucleation of small iron oxide clusters was found by TEM. The complete decomposition occurred at around 300 °C. The size of so-produced Fe_3O_4 nanoparticles could be controlled from 7 nm to 10 nm by varying the volume ratio of benzyl ether and oleylamine. As compared with the early method, the recipe is cost effective. Oleylamine is inexpensive and strong enough as a reducing agent to replace 1,2-hexadecanediol, which is more expensive.[83] In addition, the surface of so-produced Fe_3O_4 nanoparticles is only capped with oleylamine, which is believed to have a weaker bonding with the nanoparticle surface as compared with oleic acid and thus can be easily replaced by other ligands for surface modification.[84]

Alternatively, Fe-oleate complex was also reported as the precursor for large scale synthesis of high quality iron oxide nanoparticles. Hyeon *et al.* reported ultra-large scale synthesis, in which a single reaction could produce 40 g of monodisperse magnetic iron oxide nanocrystals. The method used environmentally friendly iron chloride ($FeCl_3$) and sodium oleate to prepare iron-oleate complex precursor, and then iron-oleate, oleic acid and 1-octadecene were mixed and heated up to 320 °C to synthesize iron oxide nanoparticles. The nanoparticle size could be controlled by varying reaction time, temperature, as well as the solvents with different boiling points (shown in Fig. 7). It was also concluded that the composition of iron oxide nanocrystals was Fe_3O_4 and γ-Fe_2O_3, and the Fe_3O_4 component gradually increased with the increase of the particle size.[85]

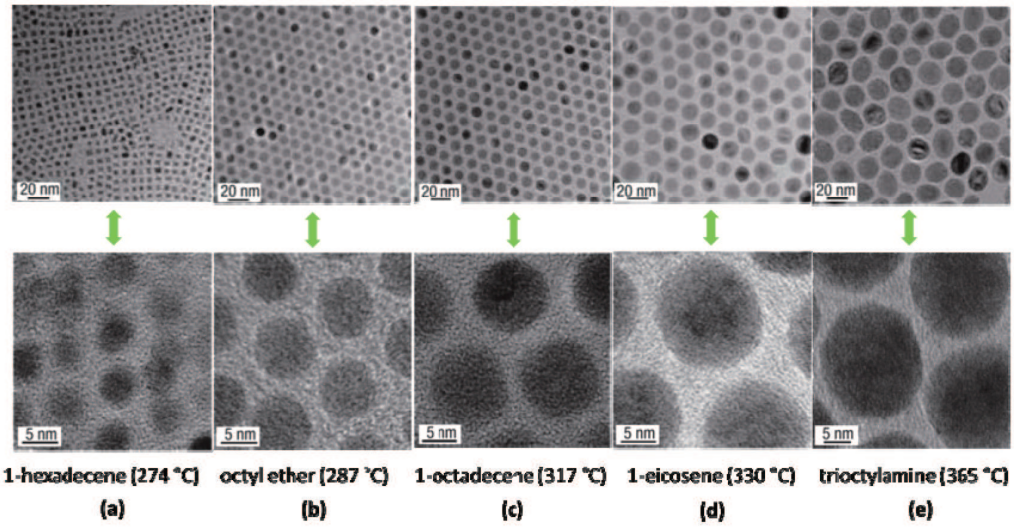


Fig. 7. TEM images and HRTEM images of monodisperse iron oxide nanocrystals synthesized using various solvents with different boiling points: (a) 5 nm; (b) 9 nm; (c) 12 nm; (d) 16 nm; and (e) 22 nm nanocrystals.[85]

$Fe(CO)_5$ can be also used as the precursor for iron oxide nanoparticles. The synthesis usually includes the formation of Fe nanoparticles from $Fe(CO)_5$ and then the oxidation into iron oxide nanoparticles. In 2007, Sun *et al.* prepared monodisperse hollow Fe_3O_4 nanoparticles by carefully controlling the oxidation process of Fe nanoparticles by $Fe(CO)_5$.[86] Because Fe nanoparticles are not chemically stable, they can be oxidized if exposed to air. The oxidation happens from the surface of Fe nanoparticles and thus the Fe/Fe_3O_4 core/shell structure can be obtained. It was found that both Fe and Fe_3O_4 were in the amorphous state. Instead of oxidation by air, controlled oxidation could be performed using the oxygen-transfer reagent trimethylamine N-oxide (Me_3NO), which resulted in a step-by-step formation of hollow Fe_3O_4 nanoparticles (as shown in Fig. 8). The controlled oxidation gave hollow Fe_3O_4 nanoparticles with polycrystalline Fe_3O_4 grains. A major advantage is that the hollow Fe_3O_4 nanoparticles are low in mass density and it may facilitate the formation of low-density porous nano-structures by self-assembly or surface functionalization. This method was modified later for the synthesis of Fe_3O_4 porous hollow nanoparticles (PHNPs) by modifying the synthesis of Fe/Fe_3O_4 nanoparticles.[11] The formation of PHNPS went through three steps. The first step was the synthesis of Fe nanoparticles. 1-octadecene, oleylamine, and $Fe(CO)_5$ was maintained at 180 °C for 30 min to produce Fe nanoparticles. The second step was to synthesize Fe_3O_4 hollow nanoparticles. It is a controlled oxidation process at different temper-

atures with different heating times. Fe nanoparticles were added to the mixture solution of 1-octadecene and trimethylamine N-oxide at 130 °C under argon gas, and then the solution experienced a series of heating processes to produce hollow Fe_3O_4 nanoparticles. Finally, the Fe_3O_4 PHNPs were synthesized by adding the hollow Fe_3O_4 nanoparticles to the mixture of oleylamine and oleic acid and then being heated and treated at 260 °C. The porous shell allowed the capsulation of the cancer chemotherapeutic drug cisplatin for controlled release. The encapsulated cisplatin was protected well from deactivation.

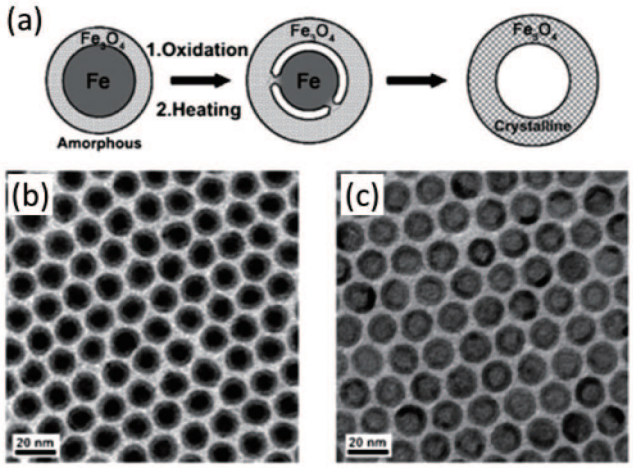


Fig. 8. (a) Synthesis of core–shell–void Fe–Fe_3O_4 and hollow Fe_3O_4 nanoparticles from Fe–Fe_3O_4 nanoparticle seeds. TEM images: (b) 13 nm Fe–Fe_3O_4 nanoparticle seeds, (c) 16 nm hollow Fe_3O_4 nanoparticles.[86]

Using $Fe(CO)_5$ as the precursor, the method can also be optimized to produce ultrasmall Fe_3O_4 nanoparticles. The nanoparticles (shown in Fig. 9) were synthesized by oxidizing the products from the thermal decomposition of iron pentacarbonyl, $Fe(CO)_5$. 4-methylcatechol (4-MC) served as the surfactant. Moreover, the 4-MC-coated Fe_3O_4 nanoparticles (shown in Fig. 23) surface could be directly conjudged with peptide, c(RGDyK), which made the nanoparticles stable in the physiology environment. The diameter of c(RGDyK)-MC-Fe_3O_4 nanoparticles is about 8.4 nm.[87]

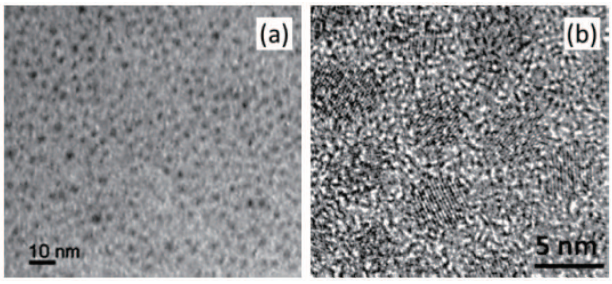


Fig. 9. (a) TEM image of 2.5 nm Fe_3O_4 nanoparticles. (b) HRTEM image of 4.5 nm Fe_3O_4 nanoparticles.[87]

Recently, Cheng *et al.* reported the synthesis of monodisperse Fe_3O_4 nanoparticles using FeO·OH as the precursor. The size of Fe_3O_4 nanoparticles could be controlled from 3 nm to 20 nm. The approach showed a large scale capability with a product mass up to 1.0 g. The synthesis was conducted by mixing FeO·OH, oleic acid, and 1-octadecene and then heating to 315 °C for 1 h. The size of so-prepared Fe_3O_4 nanoparticles has a non-monotonic change when either decreasing the precursor concentration or increasing the molar ratio of oleic acid to FeO·OH. The phenomenon could be explained as that in the "heating-up" process, the generation of monomers experienced a relatively long time and followed the nucleation and growth of the nanoparticles simultaneously. The "heating-up" process is different from "hot injection", in which "hot injection"-induced monomer supersaturation contributes to a fast homogeneous nucleation reaction. The homogeneous nucleation reaction is followed by a diffusion-controlled growth process.[88]

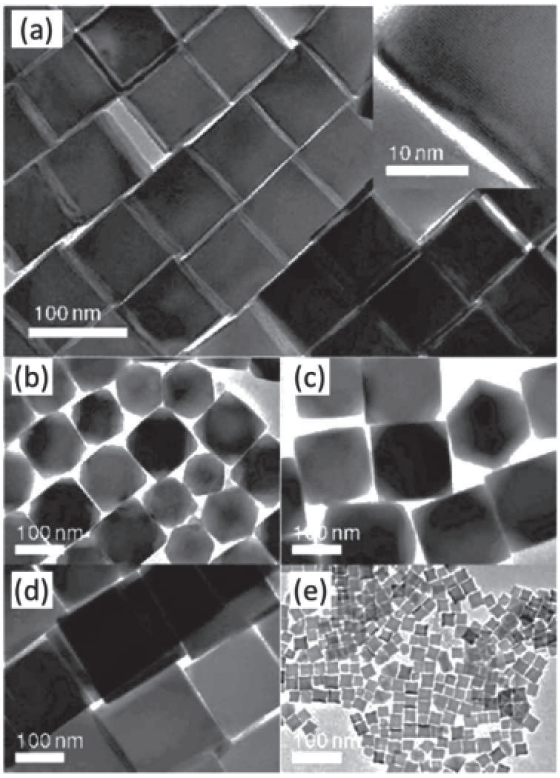


Fig. 10. TEM images of (a) 79-nm-sized Fe_3O_4 nanocubes (inset: HRTEM image); (b) mixture of truncated cubic and truncated octahedral nanoparticles with an average dimension of 110 nm; (c) 150-nm-sized truncated nanocubes; (d) 160-nm-sized nanocubes; (e) 22-nm-sized nanocubes.[25]

The thermal decomposition method also offers the shape control over iron oxide nanoparticles. In terms of the cubic shaped crystal structure, there are some reports on the synthesis of Fe_3O_4 and/or γ-Fe_2O_3 nanocubes by thermal decomposition.[25,89] Hyeon *et al.* reported the synthesis of Fe_3O_4 cubic nanoparticles using $Fe(acac)_3$ as precursor. $Fe(acac)_3$ was mixed with oleic acid and benzyl ether and then heated to 290 °C for 30 min. The reaction produced cubic-

shaped Fe_3O_4 nanoparticles with a uniform edge length of about 79 nm (Fig. 10(a)). With a reduced amount of benzyl ether, the reaction allowed the morphology evolution from the truncated cubes and truncated octahedra (Fig. 10(b)) to a perfect cubic shape (Figs. 10(c) and 10(d)). According to the HRTEM analysis, it can be concluded that the fast growth along the ⟨111⟩ direction resulted in the formation of nanocubes. The surfaces of the nanocubes were {100} planes. The synthesis also found that under high monomer concentration, the anisotropic growth was due to kinetically controlled growth. The size of nanocubes could be controlled by adding additional control agents. As 4-biphenylcarboxylic acid and oleic acid were used together, the 22 nm-sized nanocubes could be synthesized (Fig. 10(e)).[25]

Iron oxide nanocubes can also be produced using other precursors. A recent work found an interesting phenomenon that similar to some synthesis of metal nanocubes, halogen ions such as Cl and Br ions also work for the synthesis of cubic-shaped iron oxide nanoparticles in the thermal decomposition method, which has been reported by Xu *et al.*[90] Cl ions could contribute to the formation of cubic iron oxide nanocrystals (Fig. 11). When lacking of Cl ions, there were only spherical iron oxide nanocrystals. Br ions also had a similar function to control the shape of the iron oxide. The halogens played a role in stabilizing {100} facets of magnetic iron oxides, but not in regulating the thermolysis kinetics or serving as the surfactant. This method provides a new way to control the shape of iron oxide nanoparticles. It also simplified the organic phase synthesis because the metal chloride can be used directly to replace organometallic powder. So it is economical and environmentally benign.

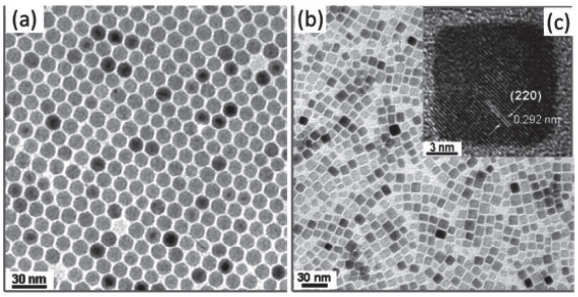


Fig. 11. (a) TEM image of spherical Fe_3O_4 nanoparticles synthesized without the presence of Cl ions. (b) TEM image of cubic Fe_3O_4 nanoparticles synthesized in the presence of Cl ions.[90]

Octahedral Fe_3O_4 nanoparticles can be synthesized using Fe-oleate, $Fe(OA)_3$ as the precursor. Hou *et al.* developed a method for shape-controlled Fe_3O_4 nanoparticles. The thermal decomposition of $Fe(OA)_3$ was conducted at a high temperature in the mixture of tetracosane and oleylamine. The lateral size of as-synthesized Fe_3O_4 octahedral nanoparticles was 21±2 nm, as shown in Fig. 12.[91]

Although high-temperature (thermal) decomposition can produce highly crystalline and uniform-sized magnetic nanoparticles by using organometallic and coordination compounds in non-polar solution,[92] there are also some limitations in this method. First, it needs relatively expensive organometallic compounds as precursors such as $Fe(CO)_5$,[93] $Fe(acac)_3$,[94] iron oleate.[95] $Fe(CO)_5$ is also very toxic. Second, the reaction process needs a high temperature and tedious procedure, which limits their large-scale production and applications.[63] Furthermore, nanoparticles applicable in biochemistry must have a hydrophilic property and can be dispersed well in water. However, the Fe_3O_4 synthesized via thermal decomposition cannot meet these demands. In addition, most bio-environments have a wide pH range (about 5–9),[76,96] where iron oxide may not be able to survive long if the pH goes lower than 7. Therefore, it is desired to optimize the surface chemistry of iron oxide nanoparticles to protect them from low pH corrosion, while functionalizing their surface for further use.

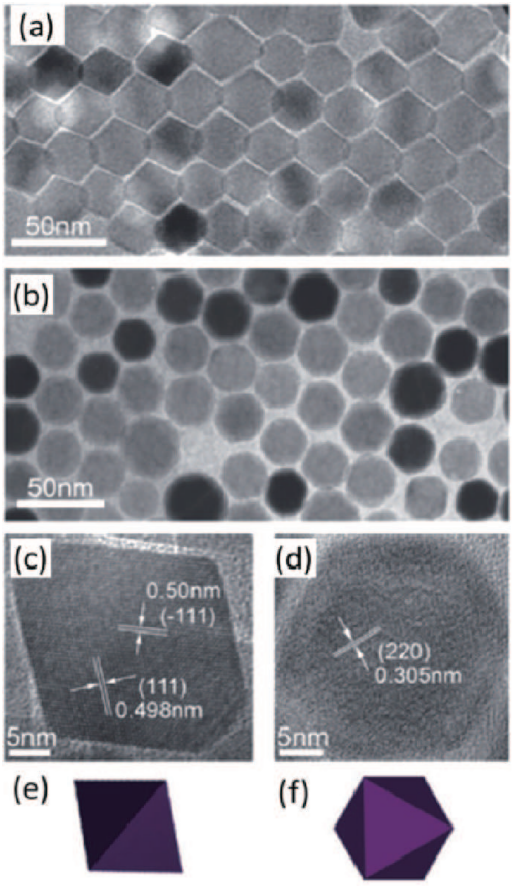


Fig. 12. TEM images of self-assembled monolayer patterns consisting of Fe_3O_4 nanoparticles with different projection axes. Image projection direction: (a) ⟨110⟩, (b) ⟨111⟩. (c) and (d) HRTEM images are projected from ⟨110⟩ and ⟨111⟩, respectively. (e) and (f) are the models of (c) and (d), respectively.[91]

5. Surface coating for biomedical application

Magnetic iron oxide nanoparticles with a bare surface tend to agglomerate because of strong magnetic attractions

among particles, the van der Waals force, and high surface energy.[79] Consequently, the agglomerated iron oxide nanoparticles can be rapidly eliminated by the reticulendothelial system (RES).[97,98] Also, a high local concentration of Fe ion from surface Fe dissolution is toxic to organisms.[99] These can be avoided by coating a shell on the iron oxide nanoparticle surface to make them hydrophilic, compatible to bio-environments, and functionalized. [33,99,100] Here we summarize several typical coating methods and materials. Some coating techniques are designed for protecting iron oxide cores from corrosion and some are designed with additional chemical and physical functions for specific applications.

5.1. Au coating

The nobel metal coating is a popular method to protect iron oxide nanoparticles from low pH corrosion. The coating with Au or Ag with surface plasmonic property is more interesting since it provides additional optical properties. As a plus, coating with Au can also facilitate the further organic conjugation by Au–S chemistry. There are many reports on the Au coating on magnetic iron oxide nanoparticles.[101–103] The coating usually is achieved by reducing Au precursor in the presence of iron oxide nanoparticles. The experimental conditions vary according to the properties of iron oxide nanoparticle cores, such as the solubility, surface chemistry, size, etc. Here we introduce some typical examples briefly. Using Fe_3O_4 nanoparticles synthesized by thermal decomposition of $Fe(acac)_3$, Xu *et al.* synthesized magnetic core/shell Fe_3O_4/Au and Fe_3O_4/Au/Ag nanoparticles by reducing $HAuCl_4$ at room temperature (shown in Fig. 13). Due to the incompatible chemistry, the coating of Au over the iron oxide surface is quite difficult. The fast reduction of Au precursor will lead to the growth of Au nanoparticles instead of coating shell. To prevent the fast reduction, the method employed oleylamine as a mild reducing agent to slowly reduce $HAuCl_4$ in chloroform solution of Fe_3O_4 nanoparticles. Also, chloroform is a strong solvent and it probably helps desorption of oleylamine, as the surfactant, from the surface of Fe_3O_4 nanoparticles, opening the surface for Au shell nucleation and growth. So-prepared Au-coated Fe_3O_4 nanoparticles were soluble in non-polar solvent because the surface was still capped by oleylamine. To make them water-soluble, these nanoparticles were dried and mixed with sodium citrate and cetyltrimethylammonium bromide (CTAB). The absorption of sodium citrate on a Au shell enabled a negative charged surface, which further led the capping of CTAB with a well-known double layer structure and a stronger capping could be achieved to replace oleylamine. The water-soluble core/shell nanoparticles could serve as seeds for thicker Au-coating by adding more $HAuCl_4$ under the reducing condition, or for Ag coating by reducing $AgNO_3$. The method not only stabilized magnetic Fe_3O_4 nanoparticles from a corrosive environment, but also manipulated the surface plasmonic absorption of magnetic core/shell nanoparticles.[103]

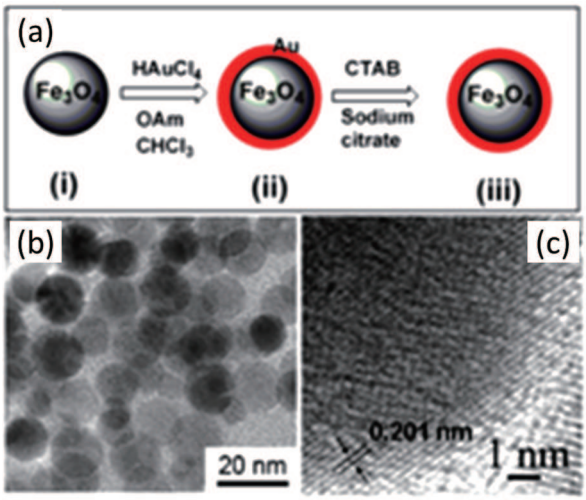


Fig. 13. (a) Schematic illustration of surface coating Fe_3O_4 nanoparticles (i) with Au to form hydrophobic Fe_3O_4/Au (ii) and hydrophilic Fe_3O_4/Au nanoparticles (iii); (b) TEM image of the nanoparticles (iii); (c) HRTEM image of part of a single Fe_3O_4/Au nanoparticle from (b).[103]

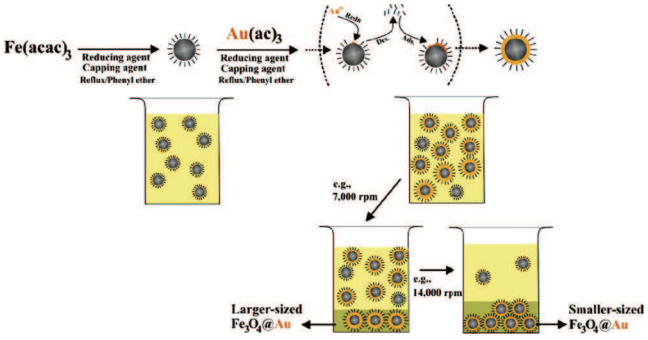


Fig. 14. Schematic illustration of the chemistry and processes involved in the synthesis of the Fe_3O_4 and Fe_3O_4@Au nanoparticles.[104]

For Fe_3O_4 nanoparticles synthesized by thermal decomposition, there is another method reported by Zhong *et al*. The schematic illustration was shown in Fig. 14.[104] The method employed $Au(Ac)_3$ as the precursor and thermally reduced this precursor at 180–190 °C in the presence of Fe_3O_4 nanoparticles. Oleic acid and oleylamine were used as surfactants and 1,2-hexadecandediol was used as the reducing agent. The desorption of oleylamine and oleic acid from Fe_3O_4 nanoparticle surfaces is facilitated by high temperature heating. The method also employed a size selection process by centrifuge to separate uncoated Fe_3O_4 nanoparticles, large-sized and small-sized core/shell nanoparticles. The shell thickness was determined by TEM and direct current plasma (DCP) composition

analysis. After coating, thiol-mediated inter-particle binding was utilized to produce a thin film of core/shell Fe_3O_4/Au nanoparticles. The thin film exhibited a similar surface plasmonic property with pure Au nanoparticle cross-linked thin films, which was used as media for gas sensor applications a few years later.

The coating of Au over the iron oxide nanoparticles by co-precipitation synthesis has also been reported with several examples. The iron oxide nanoparticles by the co-precipitation method are usually water-soluble and their surfaces are rich in OH groups. Such a surface chemistry is difficult for Au or other metal coatings. The surface modification by organic linkers is necessary. An example is to use (3-aminopropyl)triethoxysilane (APTES) to functionalize the surface with amine groups, which are affinitive to Au^{3+} ions. A small amount of HNO_3 was also used to make functionalized surface positively charged. The sonication of a mixture of APTES functionalized iron oxide nanoparticles, $HAuCl_4$, and sodium citrate finally resulted in Au-coated iron oxide nanoparticles. Li *et al.* also reported a method to modify the surface of iron oxide nanoparticles with small Au nanoparticles (Fig. 15). The difference is that the method used chemical linkers to immobilize the pre-made Au nanoparticles onto iron oxide nanoparticles. The chemical linkers are O-benzotriazole-N,N,N',N'-tetramethyluroniumhexafluorophosphate (HBTU) and triethylamine. The covalence binding between amine and OH groups linked HBTU with iron oxide nanoparticles. The thiol group on HBTU bonded with Au nanoparticles. These Au modified iron oxide nanoparticles were used for separating arginine kinase from cell lysate. The separation was achieved by applying external magnet attraction and arginine kinase persists the catalytic activity after separation.[102]

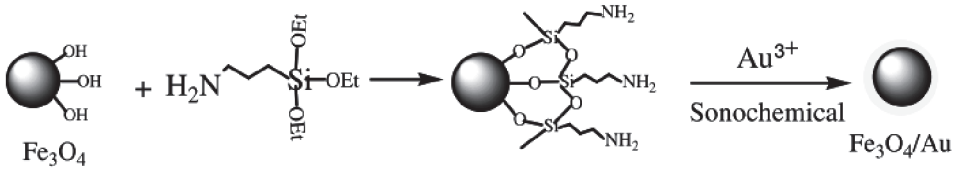


Fig. 15. Illustration of the synthetic chemistry for Fe_3O_4/Au nanoparticle preparation.[102]

5.2. SiO_2 coating

SiO_2 coating is often used in colloid surface modification. The density of silica shell can be tuned by changing reaction conditions to either porous or dense. The SiO_2 shell surface is compatible with many chemicals and molecules for further bio-conjugations.[99,105] In addition, small molecules like dye and drug, and even quantum dots can be incorporated into the silica shell during the formation of silica shell. Due to these advantages, the SiO_2 coating has been popular for magnetic iron oxide nanoparticles and a silica surface can covalently attach to various ligands and biomolecules to target organs via antibody-antigen recognition.[99,106–108] Silica coating is usually made by alkaline hydrolysis of tetraethyl orthosilicate (TEOS) in the presence of core nanoparticles. The recipe can be modified for most nanoparticles in either an organic solution or an aqueous solution. For magnetic iron oxide nanoparticles, core-shell Fe_3O_4@SiO_2 nanoparticles have been widely reported. It is interesting to note that the silica-coated iron oxide nanoparticles usually are stable and can be easily dispersed in an aqueous or organic solution, even without surfactants. Gao *et al.* used 20 nm hydrophilic Fe_3O_4 nanoparticles as seeds to prepare Fe_3O_4@SiO_2 nanoparticles , and by changing experimental conditions, the thickness of the SiO_2 shell can be tuned from 12.5 nm to 45 nm. The reaction time, the concentration of Fe_3O_4 seeds and the ratio of TEOS/Fe_3O_4 were found to be critical for controlling SiO_2 shell thickness.[99]

Xia's group reported a sol–gel method to coat iron oxide nanoparticles with silica.[109] Because the iron oxide surface has a strong affinity to silica, the coating of silica can be achieved without intermediate steps to promote the adhesion of silica to the iron oxide surface. Commercial iron oxide nanoparticles (EMG 340) dispersed in water were directly mixed with ammonium and TEOS in 2-propanol. The reaction proceeded at room temperature under stirring for 3 h. The hydrolysis of TEOS was catalyzed by ammonium hydroxide and the affinity between iron oxide and silica made silica grow over the iron oxide surface. So-produced core/shell Fe_3O_4/SiO_2 nanoparticles dispersed well in water without surfactants. The concentration ratio of iron oxide nanoparticles to TEOS had to be carefully optimized to avoid the homogeneous nucleation of silica. This ratio was also a parameter for controlling the shell thickness. They further modified the procedure by adding dye molecules to make fluorescent core/shell Fe_3O_4/SiO_2 nanoparticles. Two fluorescent dyes, 7-(dimethylamino)-4-methylcou-marin-3-isothiocyanate (DAC-ITC) and tetramethylrhodamine-5-isothiocyanate (5-TRITC), with thioisocyanate functional group were selected. The

thioisocyanate group could be coupled with amine group of 3-aminopropyl-triethoxy-silane. The covalent bond formed between the two groups stabilized the fluorescent dye molecules into the silica shell. The fluorescent core/shell Fe_3O_4/SiO_2 nanoparticles could form chain-like structures along the applied magnetic field. Due to the fluorescent dyes, they were visible under fluorescent microscopy (shown in Fig. 16).

Besides dye molecules, small nanoparticles can also be incorporated into the silica shell. Ying *et al.* incorporated quantum dots CdSe into the silica shell and produced silica coated gamma-Fe_2O_3/CdSe composite nanoparticles (shown in Fig. 17).[110] Magnetic iron oxide nanoparticles and quantum dots were firstly synthesized separately. A reverse microemulsion medium using polyoxythylene nonylphenyl ether and Igepal CO-520 was employed for controlled coating silica. The silica was produced by adding ammonium hydroxide and TEOS after dispersing iron oxide nanoparticles and quantum dots into the reverse microemulsion solution. This method successfully combined magnetic and fluorescent properties into one nanoparticle. The quantum efficiency of incorporated CdSe particles was found to be lowered as compared to bare CdSe. A thicker silica shell may further weaken the quantum efficiency. However, the magnetic saturation moment normalized by iron oxide mass persisted, without drop. The silica shell protected both iron oxide and CdSe nanoparticles and such a bi-functional nanoparticle is very promising for diagnostic imaging by either MRI or fluorescence.

Au nanoparticles with surface plasmonic absorption are also introduced into the silica-modified iron oxide nanoparticles. An example is by Hyeon *et al*. They successfully synthesized magnetic gold nanoshells (Mag-GNS), where Au and Fe_3O_4 nanoparticles formed a shell over silica nanospheres. The dense Au surface could be readily conjugated with cancer-targeting agents (Fig. 18). To immobilized Fe_3O_4 and Au nanoparticles, the surfaces of the silica spheres were firstly modified with 3-aminopropyltrimethoxysilan, which enable the surface rich in amine groups. Fe_3O_4 and Au nanoparticles were subsequently attached onto silica spheres. The further growth of Au nanoparticles resulted in a dense Au shell with Fe_3O_4 embedded. This method is quite interesting because this Au shell has NIR absorption around 700 nm. It enables the photothermal therapy against cancer cells. Additionally, magnetic Fe_3O_4 nanoparticles are well-protected into the Au shell and can be used for MRI. Lung and breast cancer cells can be clearly imaged after being targeted with these nanoparticles under T2-weighted MRI. The continuous-wave laser gives an effective local heating by the near infrared (NIR) absorption of Au shell and cancer cells can be killed under optimized power.[9]

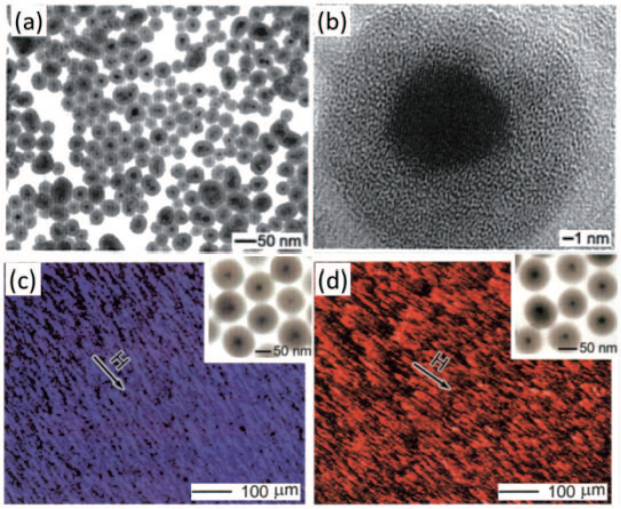


Fig. 16. (a) A typical TEM image of silica-coated Fe_3O_4 nanoparticles synthesized by the sol–gel method. (b) A close view of a single silica-coated Fe_3O_4 nanoparticle. (c) and (d) Fluorescent microscopy images of chain-like structures formed by silica-coated iron oxide nanoparticles in the presence of an external magnetic field. The silica shell was incorporated with DACITC (c) and 5-TRITC (d) with APS precursor. The insets are TEM images of core/shell Fe_3O_4/SiO_2 nanoparticles with dye molecules.[109]

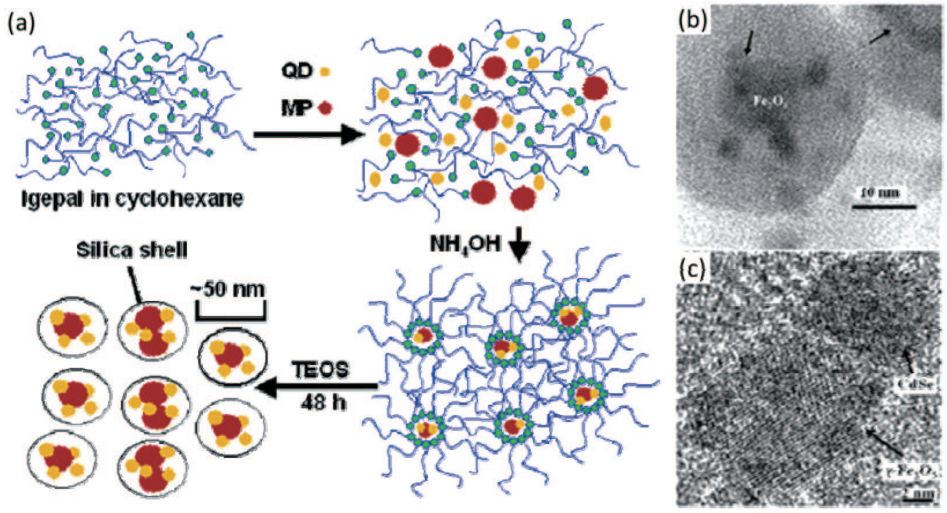


Fig. 17. (a) The procedure for synthesis of silica coated magnetic γ-Fe_2O_3 and CdSe nanoparticles. (b) The TEM image of a single core/shell nanoparticle. (c) The HRTEM image of γ-Fe_2O_3 and CdSe nanoparticles in the silica.[110]

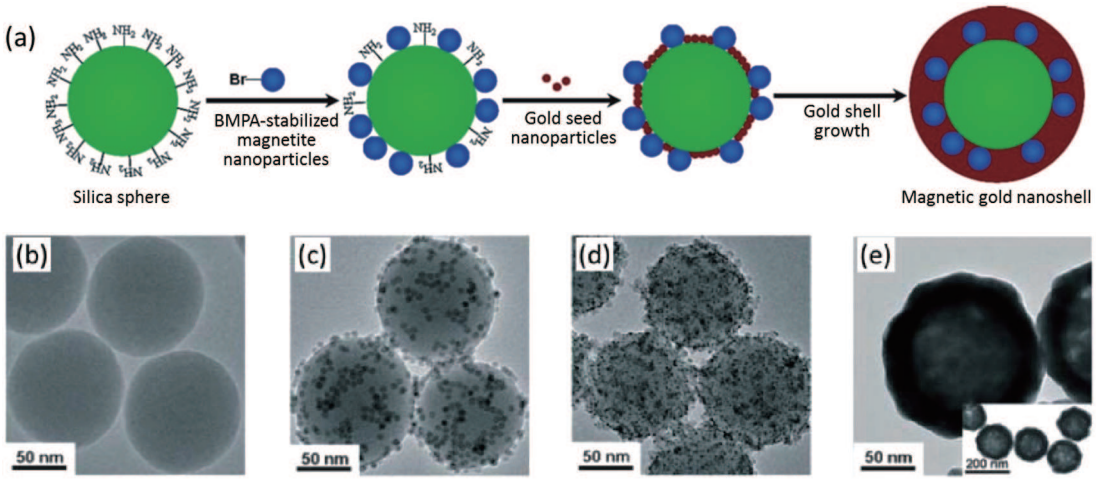


Fig. 18. (a) Synthesis of the magnetic gold nanoshells (Mag-GNS). TEM images of (b) amino-modified silica spheres, (c) silica spheres with Fe_3O_4 (magnetite) nanoparticles immobilized on their surfaces, (d) silica spheres with Fe_3O_4 and gold nanoparticles immobilized on their surfaces, and (e) the Mag-GNS.[9]

5.3. TaO_x coating

Nanosized TaO_x is a low cost CT contrast agent. It has been used for clinical applications[111,112] similar to Au[113] and Bi_2S_3.[114] Hyeon *et al.* developed core/shell Fe_3O_4/TaO_x nanoparticles as a bifunctional agent for CT and MRI (Fig. 19).[115] CT can clearly give images of newly formed blood vessels in the tumors, while MRI detects the tumor microenvironment, such as the hypoxic and oxygenated regions. The complementary information from CT and MRI provides a great potential for accurate diagnosis of cancer. The TaO_x coated Fe_3O_4 nanoparticles were synthesized by thermal decomposition of iron oleate precursor and subsequently a fast hydrolysis of tantalum ethoxide in a mixture of Igepal CO-520, NaOH, and other organic solvents. The elemental mapping image from TEM showed Fe_3O_4 was indeed coated with a thin layer of TaO_x. This shell could be made thicker if longer hydrolysis was applied. The TaO_x shell was further conjugated with rhodamine-B isothiocyanate (RITC) functionalized silane and poly(ethylene glycol) silane to enable the fluorescence capability, colloidal stability, and biocompatibility.[115,116]

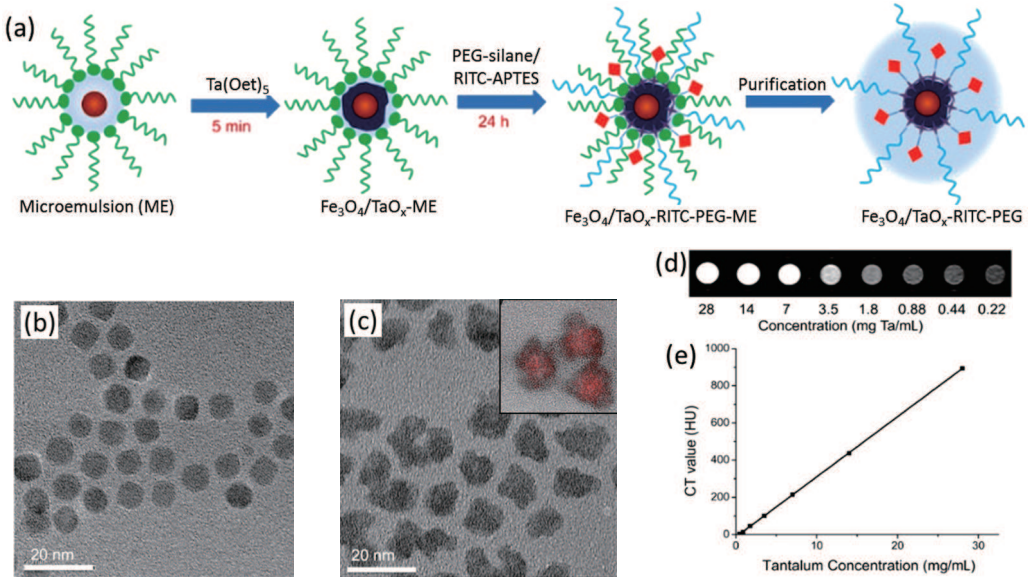


Fig. 19. (a) Schematic illustration of synthesis and modification of Fe_3O_4/TaO_x Core/Shell nanoparticles. (b) TEM image of Fe_3O_4 nanoparticles. (c) TEM image of Fe_3O_4/TaO_x Core/Shell nanoparticles. The inset is the elemental mapping image with Fe in red. (d) T phantom images at various concentrations of Fe_3O_4/TaO_x core/shell nanoparticles and (b) HU values in CT.[115]

5.4. Polymer coating

Incorporating magnetic iron oxide nanoparticles into a polymer has also been developed. Similar to silica coating, a polymer coating can also give a protective and bio-compatible organic surface for functionalization. Its synthesis is similar to the hydrolysis synthesis of silica-coated Fe_3O_4 nanoparticles, and usually they can be synthesized by polymeriza-

tion of precursors in the presence of iron oxide nanoparticles. Hyeon *et al.* developed a multifunctional polymer nanomedical platform with three functions: cancer-targeted MRI, optical imaging, and magnetically-guided drug delivery at the same time (Fig. 20). It has four parts: biodegradable poly(D,L-lactic-co-glycolic acid) (PLGA) nanoparticles served as a matrix for loading and controlling release of hydrophobic therapeutic agents into cells. Fe_3O_4 and CdSe/ZnS nanoparticles were incorporated into the PLGA matrix: Fe_3O_4 nanoparticles were used for both magnetically guided delivery and T2 MRI contrast agent, and CdSe/ZnS nanoparticles were used for optical imaging. Doxorubicin (DOXO) was used as a therapeutic agent for cancers. Finally, cancer-targeting folate was conjugated onto the PLGA nanoparticles by PEG groups to target KB cancer cells. With the increase of PLGA(MNP/DOXO) nanoparticles, the intensity of MRI singnal decreases and r2 increases. The external magnetic field during incubation can make the image darker. It also indicated that PLGA(MNP/DOXO) nanoparticles could serve as cancer-targeted, T2 contrast agents in MRI. Additionally, the combination of folate targeting groups and an external applied magnetic field could contribute to enhancing the cancer targeting efficiency.[8]

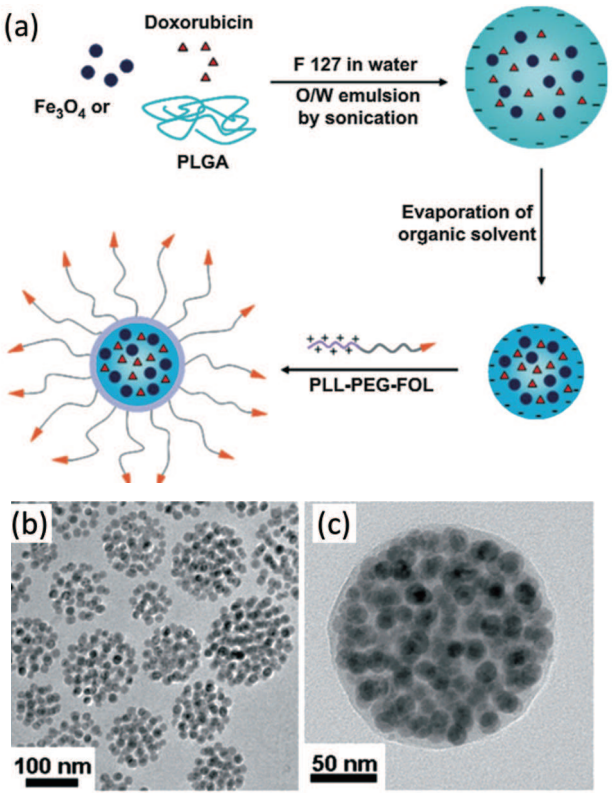


Fig. 20. (a) Synthetic procedure for the multifunctional polymer nanoparticles; (b) TEM image of PLGA(MNP/DOXO) nanoparticles embedded with 15 nm Fe_3O_4 nanocrystals; (c) a close view on a single PLGA(MNP/DOXO) nanoparticle.[8]

Polymer coatings are very popular in making colloidal nanoparticles water-soluble and biocompatible. Dextran, dendrimers, polyethylene glycol (PEG), and polyethylene oxide (PEO) are the most commonly used. As for iron oxide nanoparticles, PEG has been found to be effective to protect the iron oxide in a hydrophilic environment. PEG is an amphiphilic polymer and is commonly regarded as a non-specific interaction reducing reagent. It has been widely used for the conjugation with proteins to extend their circulation time. An early study by Sun *et al.* investigated the effect of chain length to the hydrodynamic size of PEG-capped Fe_3O_4 nanoparticles as well as the stability in buffer solutions (phosphate buffered saline (PBS)+10% fetal bovine serum (FBS)).[117] It was found that PEG could be anchored onto Fe_3O_4 nanoparticles by covalent bonding. After coating, Fe_3O_4 nanoparticles could be well-stabilized in cell culture media with negligible aggregation (Fig. 21). The non-specific uptake by macrophage cells were also found to be reduced greatly. It should be highlighted here that dopamine was used to replace the surfactants, oleic acid and oleylamine, on the surface of Fe_3O_4 nanoparticles. The dopamine moiety was proved to have a high affinity to the iron oxide surface.[118,119] Many other surface modifications have been developed based on dopamine-PEG chemistry.[120–122]

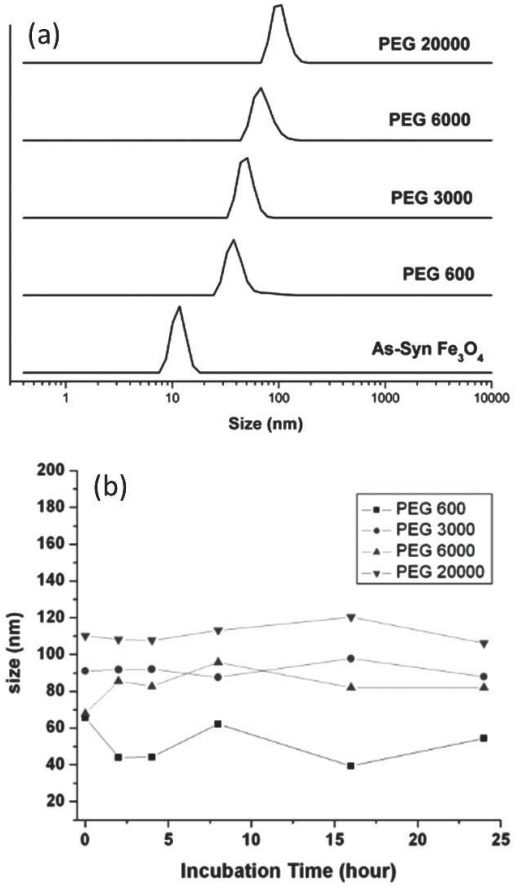


Fig. 21. (a) Hydrodynamic sizes of the Fe_3O_4 nanoparticles coated with different surfactants. The sizes were measured from the aqueous solution of the nanoparticles by dynamic light scattering (DLS). (b) Hydrodynamic size changes of the DPA-PEG coated Fe_3O_4 nanoparticles incubated in PBS plus 10% FBS at 37 °C for 24 h.[117]

Besides dopamine, phospholipid was also combined with PEG for surface modification and stabilization of iron ox-

ide nanoparticles. Hyeon *et al.* reported polyethylene glycol-phospholipid (PEG-phospholipid)-coated iron oxide nanocubes as an MRI contrast agent. Iron oxide nanocubes were synthesized via thermal decomposition of $Fe(acac)_3$ in a mixture of oleic acid and benzyl ether, and then coated with PEG-phospholipid, which could transform the hydrophobic nanoparticles to hydrophilic and biocompatible nanoparticles, and prevent extensive agglomeration. These PEG-phopholipid-coated magnetic nanoparticles were found to be capable of labeling many kinds of cells with high relaxivity.[123] However, these particles were found in low colloidal stability and the *in vivo* applications were limited. The MRI of single cells at high tesla MRI was found to be highly efficient. The use in imaging pancreatic islets at clinical MRI was also demonstrated. The imaging function of these particles persisted for nearly 150 days in pancreatic islets (Fig. 22). The work indicates that PEG based coating is a promising way to protect iron oxide from corrosion in a hydrophilic bioenvironment. The chemistry can also be varied by conjugating PEG with many active groups/molecules.

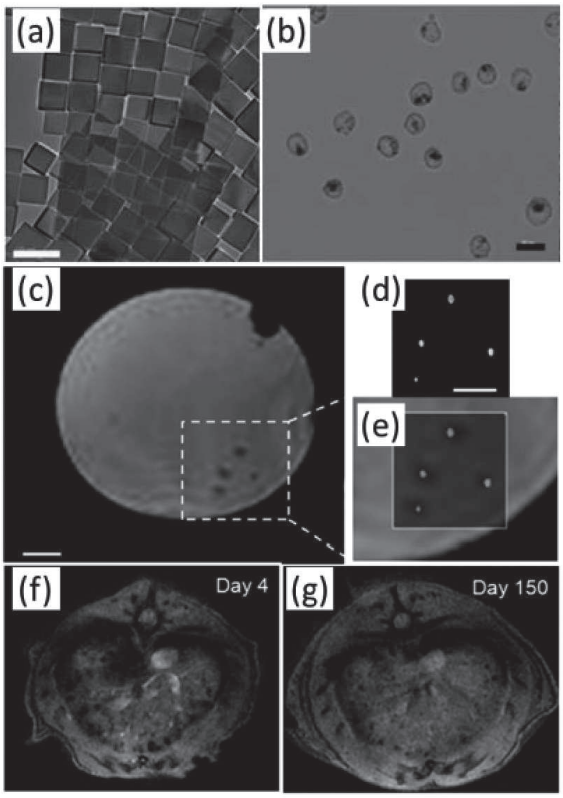


Fig. 22. (a) TEM image of iron oxide nanocubes synthesized by thermal decomposition of $Fe(acac)_3$ in a mixture of oleic acid and benzyl either (scale bar, 100 nm). These nanocubes were then capped by PEG-phospholipid through ligand exchange. (b) Trypsinized MDA-MB-231 cells. The iron oxide nanoparticles are visible as dark spots inside the cells. (c) MRI of four labeled cells sandwiched between two Gelrite layers. (d) Fluorescence image of cells stained with calcein-AM. (e) Merged image of corresponding region of (c) and (d). The dark spots in the MRI matched exactly with the green spots in the fluorescence image. *In vivo* MRI of intrahepatically transplanted syngeneic islets. T2 MRI of rat liver infused with ~3000 pancreatic islets for 4 (f) and 150 (g) days after transplantation. The hypointense spots representing labeled islet persisted up to 150 days after transplantation.[123]

Some research works tried to embed magnetic iron oxide nanoparticles into polymer hydrogels to make a "smart" platform for drug delivery. Hydrogels have been extensively studied in various biomedical applications, such as soft contact lenses, intravascular devices, wound dressings, drug delivery, and lubricants for surgical gloves. An interesting property of hydrogels is that they can swell or shrink with a volume change up to 1000 times in response to small changes in environment temperature, pH level, electric fields or solvent and ionic composition. For example, Poly (N-isopropylacrylamide) (PNIPA) hydrogel is temperature sensitive. When immersed in water, the PNIPA hydrogel has a low critical solution temperature of 34 °C. It is swollen at temperatures below 34 °C, but collapses at 34 °C and above.[124] Because of this low critical temperature for volume change in aqueous media, PNIPA hydrogel can be used for drug delivery. The drug molecules are encapsulated in the hydrogel and they can be released during this collapse transition. To generate temperature change, Ang *et al.* incorporated magnetic iron oxide particles and employed hyperthermia to increase the temperature within the PNIPA hydrogel (Fig. 23).[125] A magnetic field with a frequency of 375 kHz and the strength varying from 1.7 kA/m to 2.5 kA/m was used. The concentration of Fe_3O_4 particles was varied to investigate the temperature induced by this magnetic field. It was found that the temperature in the hydrogel induced by the magnetic field increased with the concentration of Fe_3O_4 particles. The optimal concentration was found 2.5 wt.% Fe_3O_4 in the PNIPA-Fe_3O_4 hydrogel, which took 4 min to be heated to 45 °C.

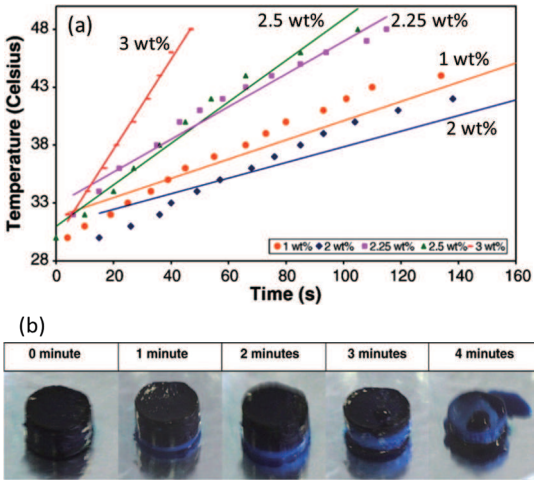


Fig. 23. (a) Temperature vs time for PNIPA-Fe_3O_4 at $H = 2.5$ kA/m. (b) Heating of PNIPA hydrogel at 34 °C as a function of time.[125]

5.5. Small molecular coating

Iron oxide nanoparticles have also been directly coated or surface-modified with small molecules to avoid a large hydrodynamic size. This is to overcome a shortcoming that the magnetic nanoparticles with a hydrodynamic size over 50 nm have a very limited extravasation ability and can be easily uptaken

by RES, which further leads to a poor targeting specificity. Xie *et al.* developed a protocol to synthesize small Fe_3O_4 nanoparticles using thermal decomposition of $Fe(CO)_5$ followed by oxidation under air. The synthesis employed 4-methylcatechol (4-MC) as the surfactant, which could be directly conjugated with a peptide, c(RGDyK), through the Mannich reaction. The protocol is illustrated in Fig. 24. The overall diameter of the c(RGDyK)-MC-Fe_3O_4 nanoparticles was about 8.4 nm, including the Fe_3O_4 core size of 4.5 nm. The c(RGDyK)-MC-Fe_3O_4 nanoparticles were stable and could target specifically to integrin $\alpha_v\beta_3$-rich tumor cells. After being accumulated preferentially in tumor cells, these nanoparticles enhanced the MRI contrast for tumor cell detection. As a plus, these RGD-coated Fe_3O_4 nanoparticles were found stable in aqueous solution for months. In addition, they proved the accumulation of c(RGDyK)-MC-Fe_3O_4 nanoparticles was mediated by integrin $\alpha_v\beta_3$ binding. Although there were some deposition seen in spleen and liver, there were rare c(RGDyK)-MC-Fe_3O_4 nanoparticles seen in kidneys and muscle, which indicated the nanoparticles could last enough circulation time for targeting.[87]

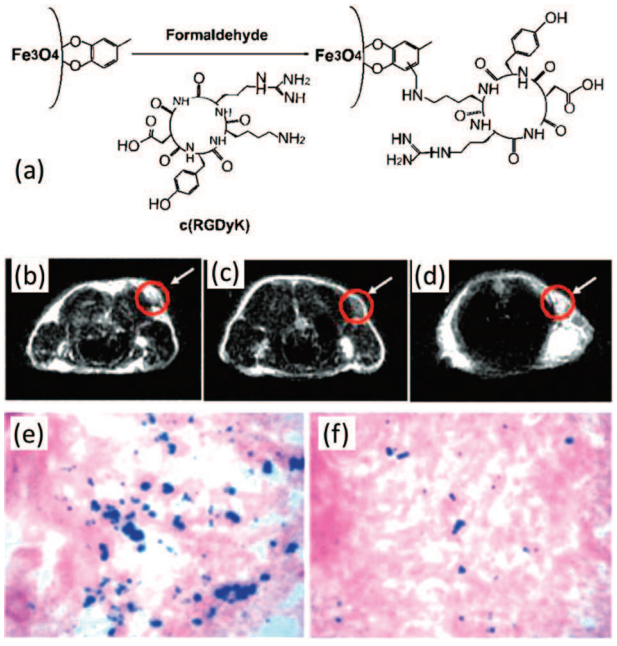


Fig. 24. (a) The protocol for producing small c(RGDyK)-MC-Fe_3O_4 nanoparticles. MRI of the cross section of the U87MG tumors implanted in mice: (b) without nanoparticles, (c) with the injection of 300 μg of c(RGDyK)-MC-Fe_3O_4 nanoparticles, and (d) with the injection of c(RGDyK)-MC-Fe_3O_4 nanoparticles and blocking dose of c(RGDyK); and Prussian blue staining of U87MG tumors in the presence of (e) c(RGDyK)-MC-Fe_3O_4 nanoparticles and (f) c(RGDyK)-MC-Fe_3O_4 nanoparticles plus blocking dose of c(RGDyK).[87]

Liposome-structured coatings were also developed for encapsulating both iron oxide nanoparticles and molecular therapeutics. A major advantage of liposomes is that it can encapsulate both hydrophobic and hydrophilic molecules very well by its closely packed phospholipid bilayer. As a result, the local dilution and the interaction with microenvironment can be prevented for encapsulated drugs. Georgy *et al.* encapsulated magnetic iron oxide nanoparticles into PEG-modified liposomes (Fig. 25).[126] The water soluble iron oxide nanoparticles were made by mechanochemical synthesis using saline crystal hydrates. The magnetic liposomes were prepared by mixing the iron oxide nanoparticles with L-a-phosphatidylcholine and 1,2-distearoyl-sn-glycero-3-phosphoethanolamine-N-[methoxy(polyethylene glycol)-2000]. These magnetic liposomes were found to be very effective to target the cathepsin inhibitor JPM-565 to the peritumoral region of mouse breast cancer, which resulted in a significant reduction in tumor growth. The work also found that magnetic liposomes could act as a drug carrier with the ability of encapsulating many different types of cargos. As a plus, iron oxide nanoparticle cores could act as an MRI contrast agent and provide the non-invasive, real time *in vivo* MRI detection.

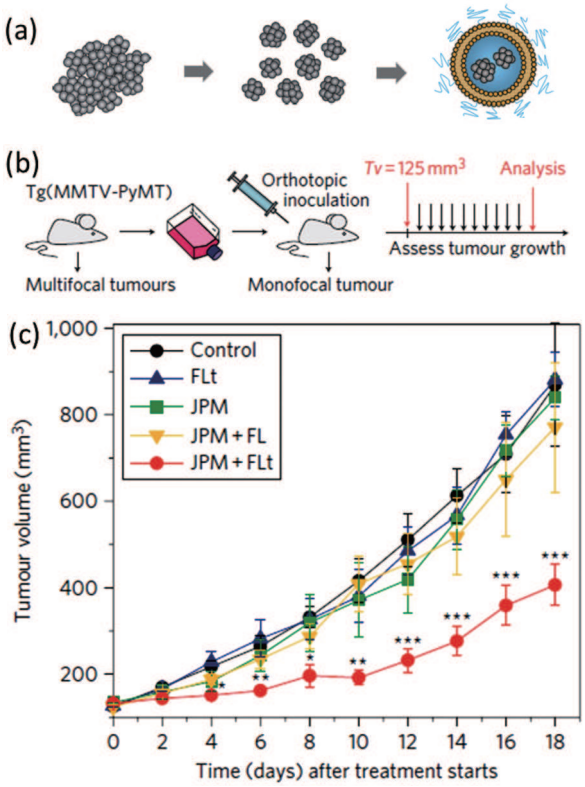


Fig. 25. (a) Preparation procedure of magnetic Fe_3O_4 liposomes. (b) Anti-tumor effect of magnetically targeted Fe_3O_4-liposomes containing cysteine protease inhibitor JPM-565. The treatment experiment with cells from the transgenic (Tg) MMTV-PyMT mouse with multifocal tumors. (c) Tumor volumes for each treatment day for the different treatment groups.[126]

5.6. Carbon coating

Carbon coating is not widely reported because the formation of carbon shell usually needs a high temperature annealing process, which carbonizes hydrocarbon precursors but will also result in the reduction of iron oxide. An example can be found in the synthesis of carboncoated FeCo

nanoparticles.[127] The synthesis was conducted by a CVD method at 800 °C under nitrogen gas protection. The precursor iron and cobalt ions were reduced to FeCo under this condition. A method to avoid this reduction is to use pre-synthesized Fe_3O_4 nanoparticles and low temperature annealing. Zhu *et al.* embedded magnetic Fe_3O_4 nanoparticles into a carbon substrate using an ethylene glycol based photoresist as the carbon source (Fig. 26).[128] They synthesized Fe_3O_4 nanoparticles by the thermal decomposition method and then used layer-by-layer assembly to make Fe_3O_4 nanoparticles embedded photoresist on a silicon substrate. The following low temperature annealing induced a carbon coated silicon substrate, where the carbon layer was embedded with Fe_3O_4 nanoparticles. Such a substrate was found to be effective for the growth of nerve cell PC12 and with the increase of Fe_3O_4 concentration, the substrate exhibited a higher adhesion ability for these cells. This approach is interesting to further studies with a combination of hyperthermia and MRI techniques for cell culture related research. Most recently, a study revealed that the Fe_3O_4 nanoparticles synthesized by the thermal decomposition method may have a thin carbon shell on their surface.[129] Iron oleate was used as the precursor and various solvents like octadecane, docosane, eicosane, and octadecene were used to adjust the thermal decomposition temperature. The highest temperature could be achieved as high as 365 °C using docosane. The work presented the evidence from HRTEM and Raman spectra, where thin carbon layers can be seen on individual Fe_3O_4 nanoparticles and D band and G band for sp^2 carbon were found. The thin carbon coating layer was probably formed by the slight carbonization of oleate ligands. These particles were tested for their cytotoxicity to several cells including HeLa Kyoto, human osteosarcoma U2OS (GFP-53BP1), NIH 3T3 fibroblasts, and Macrophages 7442. The research found that carbon coated Fe_3O_4 nanoparticles with the size range of 9.7–20.3 nm gave similar cytotoxicity results, but different uptake behaviors. The cells can uptake both single nanoparticles and small nanoparticle clusters, which may affect the evaluation of the cytotoxicity. However, the carbon coating was not found to be influential on the cytotoxicity. It is probably because the carbon coating layer was too thin to actively prevent the iron oxide from contacting with the microenvironment.

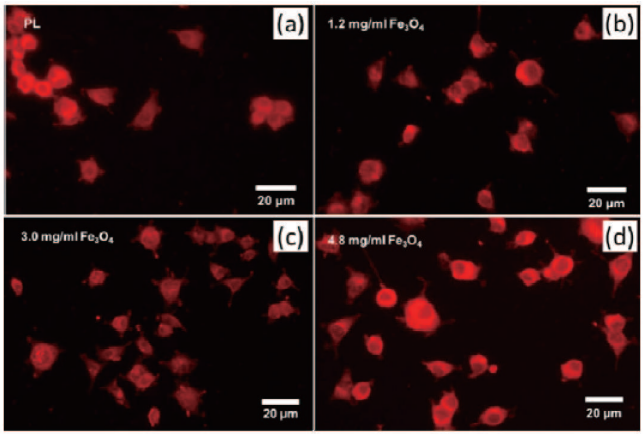


Fig. 26. Neurite length pictures of rat pheochromocytoma PC12 cells attached on carbon substrates with different Fe_3O_4 concentrations: (a) 0 mg/mL, (b) 1.2 mg/mL, (c) 3.0 mg/mL, and (d) 4.8 mg/mL.[128]

6. Conclusions and perspectives

Magnetic iron oxide nanoparticles Fe_3O_4 and γ-Fe_2O_3 have been extensively studied in terms of their synthesis approaches, characterizations, surface modifications, and biomedical applications. There are many research articles published in this field and a lot of significant progress has been made in recent years in the world wide range. This review article attempts to highlight the most popular and efficient synthesis approaches for magnetic iron oxide nanoparticles, which can be used in biomedical fields, such as MRI and drug delivery. Due to the bio-environment, iron oxide in colloidal form and soluble in an aqueous solution is a major consideration when choosing synthesis approaches. Wet-chemical approaches, such as co-precipitation in an aqueous solution and high temperature thermal decomposition of organometallic precursors, meet this criterion. Although co-precipitation can make water-soluble iron oxide nanoparticles directly, the poor crystallization and the lack of size control have limited its use. Most researchers selected thermal decomposition of organometallic precursors like $Fe(acac)_3$, $Fe(CO)_5$, and Fe-oleate to produce magnetic iron oxide nanoparticles. This method produces iron oxide nanoparticles with a high crystallization due to the high temperature employed. Involving surfactants provides a good control over the size and shape. The particles can be well-controlled into a size range from several nanometers to several decade nanometers, where they can be stabilized in colloidal form and be superparamagnetic for MRI, hyperthermia therapies, targeting cells, and drug delivery. A shortcoming of these iron oxide nanoparticles is their hydrophobic surface chemistry, which makes them only soluble in non-polar solvents like hexane and toluene. Therefore, much effort in the last few years has been made in converting their surface chemistry into hydrophilic and biocompatible. Various surface modification techniques have been developed. We summarized several typical surface modification techniques, including noble metal coating, silica coating, polymer coating, small molecular coating, and liposome coating. Indeed, to make these nanoparticles applicable in biosystems, surface modification is a critical step. It not only provides a bio-compatible surface chemistry for bio-conjugation

and functionalization, but also offers additional physical properties, such as optical and CT resonance.

To date, the synthesis approaches for magnetic iron oxide nanoparticles have been well-established. The size and shape can be controlled effectively by tuning synthetic conditions. The surface modification techniques have also been well-explored. However, the interface of nanoparticles and the bio-microenvironment is very complicated. The challenges remain in the tuning of surface chemistry of iron oxide nanoparticles. One of the future research focuses should be exploring the protocols for enhancing specific bonding for a dense functional conjugation, while lowering the non-specific bonding of unwanted biomolecules in a microenvironment. It is important to improve the targeting efficiency of iron oxide nanoparticles for tumor/cancer cells. Another issue is that exposing iron oxide into a bio-environment leads to the degradation of iron oxide nanoparticles. This will cause, for instance, the loss of MRI contrast. The dissolution of iron metal ions into the microenvironment will also result in a toxicity effect. Therefore, the techniques for building a strong, but bio-compatible surface protection layer are highly desirable. In addition, building smart structures with the abilities of diagnosis and therapeutics based on magnetic nanoparticles and other functional materials are always welcome.

References

[1] Koo B, Xiong H, Slater M D, Prakapenka V B, Balasubramanian M, Podsiadlo P, Johnson C S, Rajh T and Shevchenko E V 2012 *Nano. Lett.* **12** 2429

[2] Du X, Wang C, Chen M, Jiao Y and Wang J 2009 *J. Phys. Chem. C* **113** 2643

[3] Lin S, Shen C, Lu D, Wang C and Gao H J 2013 *Carbon* **53** 112

[4] Fukushima T, Sekizaqa K, Jin Y, Yamaya M, Sasaki H and Takishima T 1993 *Am. J. Physiol.* **265** L67

[5] Chemla Y R, Crossman H L, Poon Y, McDermott R, Stevens R, Alper M D and Clarke J 2000 *Proc. Natl. Acad. Sci. USA* **97** 14268

[6] Ugelstad J, Berge A, Ellingsen T, Schmid R, Nilsen T N, Mork P C, Stenstad P, Hornes E and Olsvik O 1992 *Prog. Polym. Sci.* **17** 87

[7] Liu Y, Gao Y and Xu C 2013 *Chin. Phys. B* **22** 097503

[8] Kim J, Lee J E, Lee S H, Yu J H, Lee J H, Park T G and Hyeon T 2008 *Adv. Mater.* **20** 478

[9] Kim J, Park S, Lee J E, Jin S M, Lee J H, Lee I S, Yang I, Kim J S, Kim S K, Cho M H and Hyeon T 2006 *Angewandte Chemie.* **118** 7918

[10] Yu J, Huang D, Yousaf M Z, Hou Y and Gao S 2013 *Chin. Phys. B* **22** 027506

[11] Cheng K, Peng S, Xu C and Sun S 2009 *J. Am. Chem. Soc.* **131** 10637

[12] Cornell R M and Schwertmann U 1996 *The Iron Oxides: Structure, Properties, Reactions, Occurrenc and Uses* (New York: VCH) pp. 6, 32, 119

[13] Ju S, Cai T Y, Lu H S and Gong C D 2012 *J. Am. Chem. Soc.* **134** 13780

[14] Mantovan R, Lamperti A, Georgieva M, Tallarida1 G and Fanciulli M 2010 *J. Phys. D: Appl. Phys.* **43** 065002

[15] Sun S and Zeng H 2002 *J. Am. Chem. Soc.* **124** 8204

[16] Yanase A and Siratori K 1984 *J. Phys. Soc. Jpn.* **53** 312

[17] Zhang Z and Satpathy S 1991 *Phys. Rev. B* **44** 13319

[18] Yang C, Wu J and Hou Y 2011 *Chem. Commun.* **47** 5130

[19] Zayachuk D M 2010 *Journal of Magnetism and Magnetic Materials* **322** 60

[20] Meyers H P *1997 Introductory Solid State Physics* (2 edn.) (New York: CRC Press) p. 362

[21] Néel L 1948 *Annales de Physique* **3** 137

[22] Arzt E 1998 *Acta Mater.* **46** 5611

[23] Wu C, Yin P, Zhu X, OuYang C and Xie Y 2006 *J. Phys. Chem. B* **110** 17806

[24] Lee N and Hyeon T 2012 *Chem. Soc. Rev.* **41** 2575

[25] Kim D, Lee N, Park M, Kim B H, An K and Hyeon T 2009 *J. Am. Chem. Soc.* **131** 454

[26] Chakraverty S and Bandyopadhyay M 2007 *J. Phys.: Condens. Matter* **19** 216201

[27] Ayyappan S, Kalyani S and Philip J 2012 *Journal of Nanofluids* **1** 128

[28] Sun S 2013 *Journal of Inorganic and Organometallic Polymers and Materials* (published online: 18 September 2013)

[29] Caravan P 2006 *Chem. Soc. Rev.* **35** 512

[30] Koenig S H and Kellar K E 1995 *Magn. Reson. Med.* **34** 227

[31] Pankhurst Q A, Connolly J, Jones S K and Dobson J 2003 *J. Phys. D: Appl. Phys.* **36** R167

[32] Muller R H and Keck C M 2004 *J. Biotechnol.* **113** 151

[33] Talelli M, Rijcken C J F, Lammers T, Seevinck P R, Storm G, Nostrum C F V and Hennink W E 2009 *Langmuir* **25** 2060

[34] Gupta A K and Ccrtis A S G 2004 *Journal of Materials Science: Materials in Medicine* **15** 493

[35] Kado T 2008 *J. Appl. Phys.* **103** 043902

[36] Ziese M and and Blythe H J 2000 *J. Phys.: Condens. Matter* **12** 13

[37] Sterbinsky G E, Cheng J, Chiu P T, Wessels B W and Keavney D J 2007 *J. Vac. Sci. Technol. B* **25** 1389

[38] Qiang Y, Antony J, Sharma A, Nutting J, Sikes D and Meyer D 2006 *Journal of Nanoparticle Research* **8** 489

[39] Yanagihara H, Myoka M, Isaka D, Niizeki T, Mibu K and Kita E 2013 *J. Phys. D: Appl. Phys.* **46** 175004

[40] Bobo J F, Basso D, Snoeck E, Gatel C, Hrabovsky D, Gauffier J L, Ressier L, Mamy R, Visnovsky S, Hamrle J, Teillet J and Fert A R 2001 *Euro. Phys. J. B* **24** 43

[41] Kumar A, Pandya D K and Chaudhary S 2012 *J. Appl. Phys.* **112** 073909

[42] Trist?ao J C, Oliveira A A S, Ardisson J D, Dias A and Lago R M 2011 *Materials Research Bulletin* **46** 748

[43] Mantovan R, Vangelista S, Cocco S, Lamperti A and Salicio O 2012 *J. Appl. Phys.* **111** 07B107

[44] Mantovan R, Lamperti A, Georgieva M, Tallarida G and Fanciulli M 2010 *J. Phys. D: Appl. Phys.* **43** 065002

[45] Vangelista S, Mantovan R, Cocco S, Lamperti A and Salicio O 2012 *Thin Solid Films* **520** 4617

[46] Carlier D, Terrier C, Arm C and Ansermet J P 2005 *Electrochemical and Solid-State Letters* **8** C43

[47] Chatman S, Noel A J G and Poduska K M 2005 *J. Appl. Phys.* **98** 113902

[48] Nishimura K, Kitamoto Y and Abe M 1999 *IEEE Trans. Magn.* **35** 3043

[49] Nikiforov M P, Vertegel A A, Shumsky M G and Switzer J A 2000 *Adv. Mater.* **12** 1351

[50] Peulon S, Antony H, Legrand L and Chausse A 2004 *Electrochim. Acta* **29** 2891

[51] Abe M 2000 *Electrochimica Acta* **45** 3337

[52] Zhu M and Diao G 2011 *The Journal of Physical Chemistry C* **115** 18923

[53] Byrappa K and Adschiri T P 2007 *Cryst. Growth Charact. Mater.* **53** 117

[54] Zhang D, Zhang X, Ni X, Song J and Zheng H 2007 *Crystal Growth & Design* **7** 2117

[55] Mu J, Chen B, Guo Z, Zhang M, Zhang Z, Zhang P, Shao C and Liu Y 2011 *Nanoscale* **3** 5034

[56] Fan N, Ma X, Liu X, Xu L and Qian Y 2007 *Carbon* **45** 1839

[57] Lu J, Jiao X, Chen D and Li W 2009 *J. Phys. Chem. C* **113** 4012

[58] Wan J, Chen X, Wang Z, Yang X and Qian Y 2005 *Journal of Crystal Growth* **276** 571

[59] Xiao Z, Xia Y, Ren Z, Liu Z, Xu G, Chao C, Li X, Shen G and Han G 2012 *Journal of Materials Chemistry* **22** 20566

[60] Cao H, Liang R, Qian D, Shao J and Qu M 2011 *Journal of Physical Chemistry C* **115** 24688

[61] Zhou S and Chen Q 2011 *Dalton Trans.* **40** 8622

[62] Muraliganth T, Murugan A V and Manthiram A 2009 *Chem. Commun.* **47** 7360

[63] Li X, Si Z, Lei Y, Tang J, Wang S, Su S, Song S, Zhao L and Zhang H 2010 *CrystEngComm.* **12** 2060

[64] Fan R, Chen X H, Gui Z, Liu L and Chen Z Y 2001 *Materials Research Bulletin* **36** 497

[65] Khollam Y B, Dhage S R, Potdar H S, Deshpande S B, Bakare P P, Kulkarni S D and Date S K 2002 *Materials Letters* **56** 571

[66] Wang J, Sun J, Sun Q and Chen Q 2003 *Materials Research Bulletin* **38** 1113

[67] Wan J, Yao Y and Tang G 2007 *Appl. Phys. A* **89** 529

[68] Duan L, Jia S, Wang Y, Chen J and Zhao L 2009 *Journal of Materials Science* **44** 4407

[69] Zhang W, Gai L, Li Z, Jiang H and Ma W 2008 *J. Phys. D: Appl. Phys.* **41** 225001

[70] Wu K T, Kuo P C, Yao Y D and Tsai E H 2001 *IEEE Trans. Magnet.* **37** 2651

[71] Liang X, Wang X, Zhuang J, Chen Y T, Wang D S and Li Y D 2006 *Adv. Funct. Mater.* **16** 1805

[72] Daou T J, Pourroy G, Begin-Colin S, Greneche J M, Ulhaq-Bouillet C, Legare P, Bernhardt P, Leuvrey C and Rogez G 2006 *Chem. Mater.* **18** 4399

[73] Wang J, Chen Q W, Zeng C and Hou B Y 2004 *Adv. Mater.* **16** 137

[74] Refait P and Genin J M R 1993 *J. Mater. Res.* **34** 797

[75] Olowe A A and Genin J M R 1991 *J. Mater. Res.* **32** 965

[76] Hui C, Shen C, Yang T, Bao L, Tian J, Ding H, Li C and Gao H J 2008 *J. Phys. Chem. C* **112** 11336

[77] Mo Z, Zhang C, Guo R, Meng S and Zhang J 2011 *Industrial & Engineering Chemistry Research* **50** 3534

[78] Kalantari K, Ahmad M B, Shameli K and Khandanlou R 2013 *Int. J. Nanomedicine* **8** 1817

[79] Xia T, Wang J, Wu C, Meng F, Shi Z, Lian J, Feng J and Meng J 2012 *CrystEngComm.* **14** 5741

[80] Yan A, Liu Y, Liu Y, Li X, Lei Z and Liu P 2012 *Materials Letters* **68** 402

[81] Liu F, Zhu J H, Hou Y L and Gao S 2013 *Chin. Phys. B* **22** 107503

[82] Hao R 2010 *Adv. Mater.* **22** 2729

[83] Xu Z, Shen C, Hou Y, Gao H and Sun S 2009 *Chem. Mater.* **21** 1778

[84] Xie J, Xu C, Xu Z, Hou Y, Young K L, Wang S X, Pourmand N and Sun S 2006 *Chem. Mater.* **18** 5401

[85] Park J, An K, Hwang Y, Park J G, Noh H J, Kim J Y, Park J H, Hwang N M and Hyeon T 2004 *Nat. Mater.* **3** 891

[86] Peng S and Sun S 2007 *Angewandte Chemie International Edition* **46** 4155

[87] Xie J, Chen K, Lee H Y, Xu C, Hsu A R, Peng S, Chen X and Sun S 2008 *J. Am. Chem. Soc.* **130** 7542

[88] Song N N, Yang H T, Ren X, Li Z A, Luo Y, Shen J, Dai W, Zhang X Q and Cheng Z H 2013 *Nanoscale* **5** 2804

[89] Yang H, Ogawa T, Hasegawa D and Takahashi M 2008 *J. Appl. Phys.* **103** 07D526

[90] Xu Z, Shen C, Tian Y, Shi X and Gao H J 2010 *Nanoscale* **2** 1027

[91] Zhang L, Wu J, Liao H, Hou Y and Gao S 2009 *Chem. Commun.* **29** 4378

[92] Rockenberger J, Scher E C and Alivisatos A P 1999 *J. Am. Chem. Soc.* **121** 11595

[93] Casula M F, Jun Y W, Zaziski D J, Chan E M, Corrias A and Alivisatosand A P 2006 *J. Am. Chem. Soc.* **128** 1675

[94] Li Z, Chen H, Bao H B and Gao M Y 2004 *Chem. Mater.* **16** 1391

[95] Jana N R, Chen Y and Peng X G 2004 *Chem. Mater.* **16** 3931

[96] Robinson D B, Persson H H J, Zeng H, Li G, Pourmand N, Sun S H and Wang S X 2005 *Langmuir* **21** 3096

[97] Jain T K, Reddy M K, Morales M A, Leslie-Pelecky D L and Labhasetwar V 2008 *Mol .Pharmaceutics* **5** 316

[98] Neuberger T, Schopf B, Hofmann H, Hofmann, M and Von R B 2005 *J. Magn. Magn. Mater.* **293** 483

[99] Hui C, Shen C, Tian J, Bao L, Ding H, Li C, Tian Y, Shi X and Gao H J 2011 *Nanoscale* **3** 701

[100] Lu Y, Yin Y D, Mayers B T and Xia Y N 2002 *Nano Lett.* **2** 183

[101] Wang L, Park H Y, Lim S I I, Schadt M J, Mott D, Luo J, Wang X and Zhong C J 2008 *Journal of Materials Chemistry* **18** 2629

[102] Wu W, He Q, Chen H, Tang J and Nie L 2007 *Nanotechnology* **18** 145609

[103] Xu Z, Hou Y and Sun S 2007 *J. Am. Chem. Soc.* **129** 8698

[104] Wang L, Luo J, Fan Q, Suzuki M, Suzuki I S, Engelhard M H, Lin Y, Kim N, Wang J Q and Zhong C J 2005 *J. Phys. Chem. B* **109** 21593

[105] Morel A L, Nikitenko S I, Gionnet K, Wattiaux A, Lai-Kee-Him J, Labrugere C, Chevalier B, Deleris G, Petibois C, Brisson A and Simonoff M 2008 *ACS Nano* **2** 847

[106] Ulman A 1996 *Chem. Rev.* **96** 1533

[107] Gritti F and Guiochon G 2006 *J. Chromatogr. A* **1132** 51

[108] Sieburth S M and Fensterbank L 1993 *J. Org. Chem.* **58** 6314

[109] Lu Y, Yin Y, Mayers B T and Xia Y 2002 *Nano Lett.* **2** 183

[110] Yi D K, Selvan S T, Lee S S, Papaefthymiou G C, Kundaliya D and Ying J Y 2005 *J. Am. Chem. Soc.* **127** 4990

[111] Bonitatibus P J, Jr, Torres A S, Kandapallil B, Lee B D, Goddard G D, Colborn R E and Marino M E 2012 *ACS Nano* **6** 6650

[112] Oh M H, Lee N, Kim H, Park S P, Piao Y, Lee J, Jun S W, Moon W K, Choi S H and Hyeon T 2011 *J. Am. Chem. Soc.* **133** 5508

[113] Popovtzer R, Agrawal A, Kotov N A, Popovtzer A. Balter J, Carey T E and Kopelman R 2008 *Nano Lett.* **8** 4593

[114] Ai K, Liu Y, Liu J, Yuan Q, He Y and Lu L 2011 *Adv. Mater.* **23** 4886

[115] Lee N, Cho H R, Oh M H, Lee S H, Kim K, Kim B H, Shin K, Ahn T Y, Choi J W, Kim Y W, Choi S H and Hyeon T 2012 *J. Am. Chem. Soc.* **134** 10309

[116] Ling D and Hyeon T 2013 *Small* **9** 1450

[117] Xie J, Xu C, Kohler N, Hou Y and Sun S 2007 *Adv. Mater.* **19** 3163

[118] Marcelo G, Muñoz-Bonilla A, Rodríguez-Hernández J and Fernández-García M 2013 *Polymer Chemistry* **4** 558

[119] Shultz M D, Reveles J U, Khanna S N and Carpente E E 2007 *J. Am. Chem. Soc.* **129** 2482

[120] Schladt T D, Schneider K, Shukoor M, Natalio F, Bauer H, Tahir M N, Weber S, Schreiber L M, Schröder H C, Müller W E G and Tremel W 2010 *Journal of Materials Chemistry* **20** 8297

[121] Lee H, Dellatore S M, Miller W M and Messersmith P B 2007 *Science* **318** 426

[122] Latham A H and Williams M E 2008 *Acc. Chem. Res.* **41** 411

[123] Lee N, Kimb H, Choi S H, Park M, Kim D, Kim H C, Choi Y, Lin S, Kim B H, Jung H S, Kim H, Parkc K S, Moon W K and Hyeon T 2011 *Proc. Natl. Acad. Sci. USA* **108** 2662

[124] Kim S J, Lee C K, Lee, Y M and Kim and Sun I 2003 *Journal of Applied Polymer Science* **90** 3032

[125] Ang K L, Venkatraman S and Ramanujan R V 2007 *Materials Science and Engineering: C* **27** 347

[126] Mikhaylov G, Mikac U, Magaeva A A, Itin V I, Naiden E P, Psakhye I, Babes L, Reinheckel T, Peters C, Zeiser R, Bogyo M, Turk V, Psakhye S G, Turk B and Vasiljeva O 2011 *Nat. Nanotechnol.* **6** 594

[127] Seo W S, Lee J H, Sun X, Suzuki Y, Mann D, Liu Z, Terashima M, Yang P C, McConnell M V, Nishimura D G and Dai H 2006 *Nat. Mater.* **5** 971

[128] Zhu Z, Rezhdo O, Perrone M, Bao Z, Munir A, Wang J, Zhou H S and Shao J 2013 *Colloids Surf. B: Biointerfaces* **102** 428

[129] Mendes R G, Koch B, Bachmatiuk A, El-Gendy A A, Krupskaya Y, Springer A, Klingeler R, Schmidt O, Buchner B, Sanchez S and Rummeli M H 2014 *Biochim Biophys. Acta* **1840** 160